Chapter 5

Active Solvent Hydrogen Enhanced Catalytic Reduction of p-Nitrophenol using Binary and Ternary Silver Nanocomposites and its Antibacterial Action

5.1. Introduction

Heterogeneous catalysis has tremendous applications in many organic transformations, as seen in many industrial and academic research.[1-7] Heterogeneous transition metal nanocatalysts have attracted significant attention because of their mild reaction conditions, recyclability, enhanced catalytic performance, and simple separation strategies.[8-21] Among different transition metal nanocatalysts, silver nanoparticles, in particular, possess special features such as easiness of synthesis, good catalytic activity, remarkable electrical and optical properties, less toxicity and cost effectiveness.[22-24] Silver nanoparticles could function as stable nanocatalysts for desired applications via stabilizing them with capping molecules, surfactants, and polymer matrices.[22,25,26] Heterogeneous catalysts have good prospects in recovery and reusability than homogeneous catalysts. However, the former inherently exhibits poor solubility/dispersibility.[27, 28] Bare colloidal nanoparticles have an aggregation effect with time which reduces catalytic activity with storage.[8, 9] Besides that, colloidal nanoparticles require a tedious process to purify from the mother liquid. In contrast, heterogeneous catalysts can be purified by simple washing and filtration. Moreover, the irreversible nature of homogeneous silver colloidal systems restricts them to single catalytic use. Therefore, facile, green, and cost-effective metal nanoparticle-supported heterogeneous nanocomposites with good dispersibility in water or other solvents deserve immense attention in recent times. Lee and co-workers studied silver

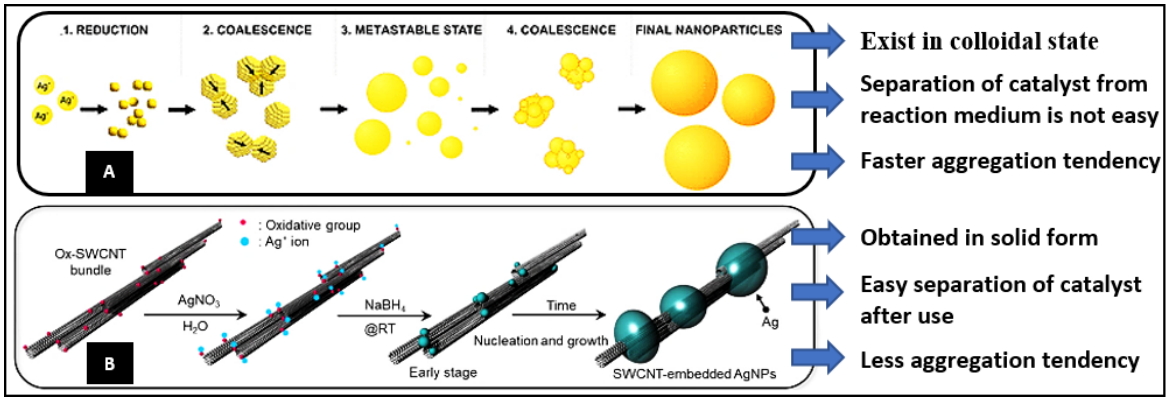

Figure 5.1. *Illustration of formation of colloidal silver nanoparticles without having host material (A) and formation of CNT-hosted silver nanoparticles (B) (Adapted from Lee et al. 2021).*

nanoparticles embedded in single-walled carbon nanotube nanocomposites for wearable electronics and sensor applications in which carbon nanotubes function as hosts for silver nanoparticles against agglomeration (see **Figure 5.1.**).[29] Polymer/carbon nanomaterial

hosted metal nanocatalysts have been recognized as green catalysts because of the energy benefits in catalytic use and catalytic recyclability without significant loss of nanoparticles.[30] The polyelectrolyte-carbon nanotube host system nanocomposites could provide good dispersibility, charged cationic or anionic side chains, and mechanical stability.[30] Conducting polymers were recently used for the preparation of conducting polymer-multiwalled carbon nanotube nanocomposites by in situ polymerization. Conducting polythiophene-MWCNT nanocomposites have high electrical conductivity, good optical properties, biocompatibility, environmental/thermal stability, and better host interactions with metal nanoparticles.[31] The stability of metal nanoparticles against oxidation, agglomeration and leaching from the supporting framework remained as the critical issues to be addressed for the performance of heterogeneous polymer/carbon nanomaterial supported metal nanocatalysts.[28-35]

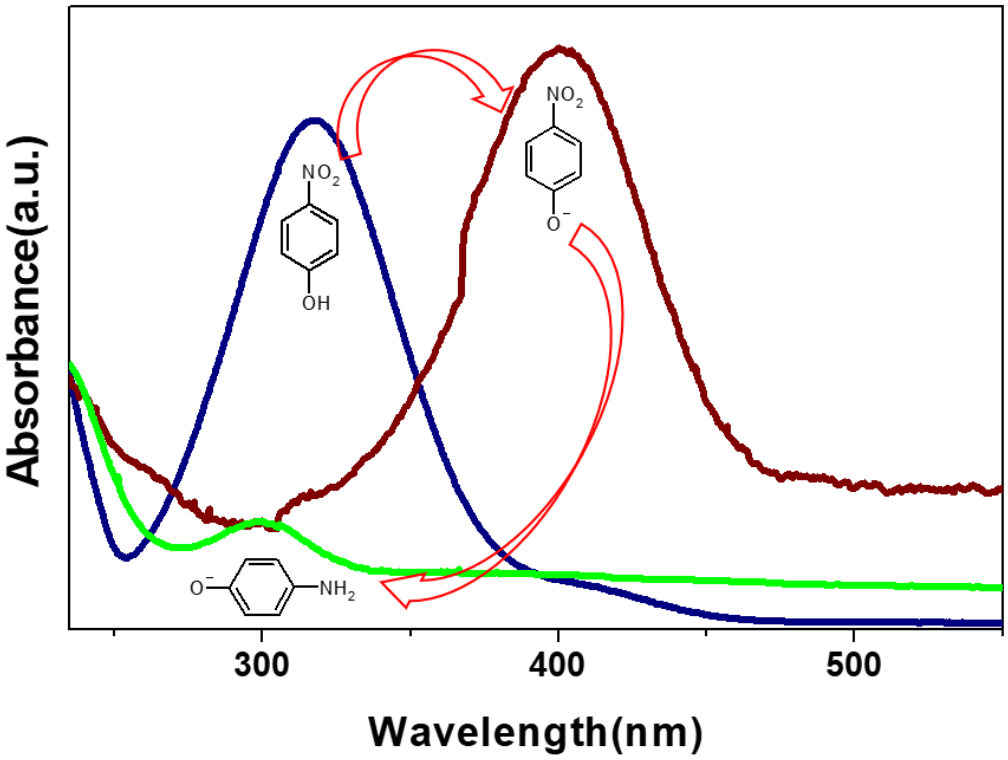

Figure 5.2. *UV-Vis spectra of p-nitrophenol, p-nitrophenolate ion and reduced product p-amino phenolate ion by adding a reducing agent and a suitable catalyst.*

Catalytic reduction of p-nitrophenol using sodium borohydride as a hydride source in the presence of different nanocatalysts is considered as a typical model reaction due to mild reaction conditions, moderate reaction kinetics, and simple experimental setup.[36-38] The changes that occurred in UV-vis spectra in different stages during the catalytic

reduction of p-nitrophenol is shown in **Figure 5.2.** The high reaction rate was not achieved until we used an excessive sodium borohydride to exhibit pseudo-first-order and more than the minimum quantity as a catalyst. Therefore, catalytic reduction of p-nitrophenol requires some reaction conditions improvements to obtain enhanced catalytic conversion with minimum reagents and catalyst (see **Figure 5.3.**). Acceleration of the reaction kinetics with some metal salts or other reagents has been conducted previously in the literature.[39-42] The mechanism of the catalytic reduction of p-nitrophenol for substantiating the source of hydrogens remains ambiguous.[39,43-47] Recently, Zhao et al. investigated the catalytic reduction of p-nitrophenol with sodium borohydride using a deuterium isotope experiment. Their work substantiated the requirement of polar protic solvents, and it acts as the source of hydrogen rather than a hydride reducer.[43] Fountoulaki et al. studied kinetic isotope effects on catalytic reduction of p-nitrophenol using $NaBH_4$ and $NaBD_4$, which has given evidence for B-H bond cleavage at rate-determining step and in-situ formation of Au-H.[44] More validating evidence is required to understand the role of water and other protic solvents for the hydrogenation of p-nitrophenol.

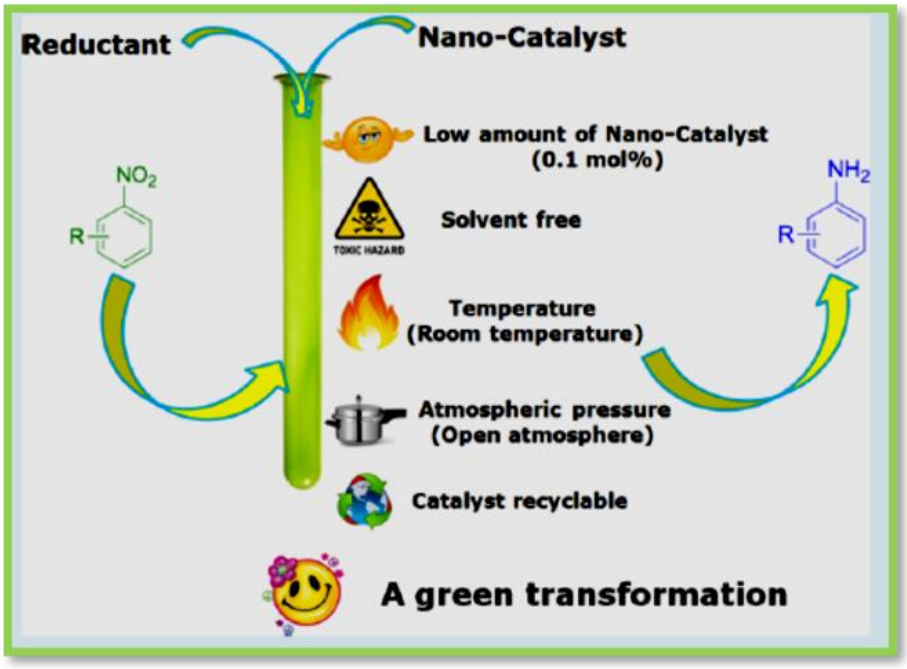

Figure 5.3. *Accounting the benefits of nanocatalysts in model nitrophenol reduction reaction (adapted from Bhairi et al. 2018)*

The present chapter focuses on the reduction reaction of p-nitrophenol to p-aminophenol in the presence of ternary (TNC) and binary nanocatalysts (BNC); both

contain silver nanoparticles embedded on different hosts, polythiophene-functionalized multiwalled carbon nanotubes nanocomposite, and functionalized multiwalled carbon nanotubes, respectively. The kinetics of binary silver nanocatalyst ($k = 0.0364\ s^{-1}$) were two to three times faster than ternary nanocatalyst ($k = 0.0134\ s^{-1}$). The optimum nanocatalyst concentration for reducing p-nitrophenol at concentration 1×10^{-4} M was determined to be 0.06 mg/mL. We have carried out the reaction kinetics of nitrophenol in polar protic and aprotic solvents miscible with water. The glycerol-water mixture (5%-30%) acts as energizing solvent for nitrophenol reduction with $NaBH_4$. By employing a green solvent combination of 10% glycerol, the catalytic activity factor enhanced to 936.50 $s^{-1}g^{-1}$ (3 times higher activity than in water as solvent); therefore, we could reduce catalyst concentration and sodium borohydride concentration approximately to one-sixth. A plausible mechanism demonstrated for the nitrophenol reduction using sodium borohydride and active hydrogens in the solvent. Ternary silver nanocatalyst has shown better dispersion than binary nanocatalyst, which lead us to study the antimicrobial properties. The ternary nanocomposites with a lower atomic percentage of silver nanoparticles was attached to the less cytotoxic polythiophene layer act as an efficient antibacterial agent against *Escherichia coli* bacteria.[48-50] In summary, binary silver nanocatalyst (BNC) functioned as an efficient catalyst for reducing p-nitrophenol, whereas ternary nanocatalyst (TNC) acts as excellent antibacterial material against *Escherichia coli* bacteria in solution.[51-56]

5.2. Experimental

5.2.1. Materials and reagents: Sodium borohydride was purchased from Sigma Aldrich. Para-nitrophenol was purchased from LOBA chemicals. Para-aminophenol was purchased from NICE chemicals. Acetone, glycerol (anhydrous), ethylene glycol, and 1,4-dioxane were purchased from Merck chemicals, India. Deionized water was used as a solvent in catalysis and for nutrient broth preparation (a mixture of peptone, NaCl, and yeast extract from NICE chemicals and beef extract from Merck chemicals, India).

5.2.2. Measurements and Instruments: UV-vis absorption spectra of the samples were recorded by Shimadzu UV-VIS spectrophotometer, UV 1800 series in the range 250-500 nm with deionized water. The powder wide-angle X-ray diffraction of the samples was measured using PANALYTICAL, Aeris research X-ray diffractometer with 2θ values ranging from 10 to 80°. Field emission scanning electron microscopy (FE-SEM) and EDX

element mapping images were recorded using ZEISS ΣIGMA^{TM}. XPS analysis was conducted using PHI 5000 Versa Probe II, ULVAC-PHI Inc, USA X-ray photoelectron spectrometer. Optical densities of E. coli inoculated samples were recorded in an antibacterial assay using AU2701 UV-VIS double beam spectrophotometer, systronics.

5.2.3. Reaction kinetics using different nanocatalyst concentrations: Different concentrations of ternary silver nanocatalysts (TNCs) were prepared by dispersing 0.5 mg, 1.0 mg, 1.5 mg and 2.5 mg of TNCs in p-nitrophenol solution (25 mL, 1.0 $\times 10^{-4}$ M) via sonication to obtain 0.02 mg/mL, 0.04 mg/mL, 0.06 mg/mL and 0.10 mg/mL respectively. The respective concentrations abbreviated as TNC-0.02, TNC-0.04, TNC-0.06, and TNC-0.10, where the figures show the concentrations in mg/mL. Similarly, binary nanocatalysts (BNCs) designated as BNC-0.02, BNC-0.04, BNC-0.06, and BNC-0.10 for same concentrations.

A typical procedure is showed below to determine the reaction kinetics using nanocatalyst concentration TNC-0.06. Ternary nanocatalyst TNC (1.5 mg) was dispersed in p-nitrophenol (25 mL, 1.0 $\times 10^{-4}$ M) by sonication for 15 min. Freshly prepared $NaBH_4$ solution (2 mL, 1.0 $\times 10^{-1}$ M) was added to 2 mL of a sonicated mixture of p-nitrophenol and TNC (0.06 mg/mL) taken in a vial, after that shaken for 10 s. We have mixed p-nitrophenol-nanocatalyst reaction mixture and sodium borohydride solution in equal volume for all catalytical studies, therefore the final concentrations of p-nitrophenol, sodium borohydride, and nanocatalyst reduced to half (**Table 5.1.**). UV-vis absorption spectra were recorded automatically in regular intervals of time by the preset program. UV-vis absorption spectra of p-nitrophenol reduction using different nanocatalyst concentrations TNC-0.02, BNC-0.02, TNC-0.04, BNC-0.04, BNC-0.06, TNC-0.10, and BNC-0.10 were recorded using the same reaction conditions. The rate constants were calculated from the linear fit plots of UV-vis absorbance of the final mixture.

5.2.4. Recycling studies using nanocatalysts: TNC (7 mg) was dispersed in p-nitrophenol solution (5 mL, 2.33 $\times 10^{-3}$ M) by sonication for 15 min. Freshly prepared $NaBH_4$ solution (5 mL, 2.33 M) was added to the above mixture. The reaction mixture was shaken well for one minute, then kept undisturbed for 10 min, and centrifuged. After centrifugation for three min, filtrate decanted, and then UV-vis absorption spectra were recorded. The residue (nanocatalyst) was washed with deionized water, and catalytical activities continued for four more consecutive cycles using the same method. A similar

procedure was repeated using BNC nanocatalyst (7 mg) instead of TNC for six catalytic cycles.

5.2.5. Recycling effects of nanocatalysts on morphology and composition: The nanocatalyst TNC (25 mg) was dispersed in p-nitrophenol solution (25 mL, 1.66 $\times 10^{-3}$ M) by sonication for 15 min. Freshly prepared $NaBH_4$ solution (25 mL, 1.66 M) was added and shaken well for one minute to the above mixture. It was kept undisturbed for 10 min to complete the reaction and then filtered. The nanocatalyst residue obtained was again dispersed in p-nitrophenol solution (25 mL, 1.66 $\times 10^{-3}$ M) and repeated the process up to the 9^{th} cycle in the same manner. After the third, sixth, and ninth catalytic cycles, a portion (one-third of the initial amount of catalyst) of the residue was separated and centrifuged to recover the catalyst. The residue was washed with water and acetone, then dried in a vacuum oven at 60°C for 1 hour. The morphology and composition of nanocatalysts recorded using powder X-ray diffraction, X-ray photoelectron spectroscopy, and scanning electron microscopy. The same procedure was repeated using BNC nanocatalyst to find any difference in morphology and composition.

5.2.6. TNC catalyzed reduction in different volume percentages of glycerol-water mixtures: TNC (1.5 mg) was dispersed in p-nitrophenol solution (25 mL, 1.0 $\times 10^{-4}$ M) by sonication for 15 min. $NaBH_4$ solution (5 mL) prepared in different volume percentages of the glycerol-water mixture was added to the P-NP-TNC mixture (5 mL) taken in different vials. The final percentage volumes of glycerol in water were 5% v/v, 10% v/v, 20% v/v, 30% v/v, 40% v/v and 50% v/v. The time for reaction completion was obtained from the change in colour of the reaction mixture from greenish-yellow to colourless. The same procedure was repeated for BNC catalyzed reduction of p-nitrophenol in different volume percentages of solvent mixtures. The other solvent mixtures such as ethylene glycol in water, ethanol in water, and 1, 4-dioxane in water were similarly used as solvent media for catalytic reduction of P-NP using nanocatalysts.

5.2.7. Calibration curve of 4-aminophenolate to find the relative yield of product: Different concentrations of p-aminophenol (5×10^{-4} M, 1×10^{-4} M, 5×10^{-5} M, 1×10^{-5} M, 5×10^{-6} M, 1×10^{-6} M, 5×10^{-7} M, 1×10^{-7} M) were taken in 10 mL deionized water. Freshly prepared $NaBH_4$ solution (10 mL, $1x10^{-1}$ M) is added to each concentration of p-aminophenol. UV-vis spectra of all above concentrations were recorded to get a calibration

curve and it can be used to quantify the concentration of p-aminophenol formed in unknown samples.

5.2.8. Large scale reduction of p-nitrophenol: Binary nanocatalyst BNC (1.8 mg) was dispersed in 10 mL p-nitrophenol solution (0.15 g, 0.108 M, 15 g/L) and sonicated for 15 min. To this $NaBH_4$ solution (10 mL, 2.695 M, P-NP: $NaBH_4$ molar ratio is 1:25) freshly prepared in 10% glycerol-water mixture was added and magnetically stirred for one hour. The completion of the reaction was observed from the colour change of greenish yellow colour of p-nitrophenol to the colourless p-aminophenolate product in one hour. Completion of the reaction was also monitored by recording UV-vis spectra of colourless p-aminophenolate product formed after one hour.

5.2.9. Antibacterial study using ternary nanocatalyst TNC: The nutrient broth was prepared by dissolving NaCl (0.5 %), peptone (0.5 %), beef extract (0.3 %) and yeast extract (0.3 %) in double-distilled water. The pH was adjusted to 7.4 and sterilized by autoclaving at 15 lbs pressure (121°C) for 15 min. The stock solution of dispersed TNC (200 µg/mL) was prepared in 50 mL nutrient broth by sonication for 30 min. Different concentrations of TNC nanocatalyst such as 1×10^{-1} µg/mL, $5x10^{-1}$ µg/mL, 1 µg/mL, 5 µg/mL, 10 µg/mL, 20 µg/mL, 30 µg/mL, 40 µg/mL, 80 µg/mL, 120 µg/mL, 160 µg/mL were prepared by adding 5 µL, 25 µL, 50 µL, 250 µL, 500 µL, 1000 µL, 1500 µL, 2000 µL, 4000 µL, 6000 µL and 8000 µL of stock solution (200 µg/mL) to nutrient broth to obtain 10 mL of total volume. The stock solution also took for antibacterial activity.

Samples containing broth mixtures were sonicated for 10 min. All tubes were inoculated with 50 µL of actively growing E. coli culture and incubated overnight in a thermal shaker at 37 ºC. After incubation, microbial growth in each tube was studied using a UV-vis double beam spectrophotometer by measuring optical density at 660 nm. Positive and negative controls were used to validate the results.

The same experiment was repeated using lactose broth instead of nutrient broth. The preparation of lactose broth is as follows: lactose (0.5 %), peptone (0.5 %) and beef extract (0.3 %) were dissolved in 1 L of double distilled water. The pH was adjusted to 6.9 and sterilized by autoclaving at 15 lbs pressure (121 °C) for 15 min.

5.3. Results and Discussion

5.3.1. Comparison of TNC and BNC nanocatalysts

Silver nanoparticles embedded ternary nanocatalyst (TNC) and binary nanocatalyst (BNC) were obtained by reducing silver nitrate solution using ascorbic acid as a reducing agent. Polythiophene-functionalized MWCNT nanocomposites and functionalized multiwalled carbon nanotubes were used as host materials for silver nanoparticles in TNC and BNC. Functionalization of multiwalled carbon nanotube was achieved by refluxing MWCNT (0.40 g) with nitric acid (5 M, 50 mL) at 100ºC. Functionalization of multiwalled carbon nanotubes reduces the aggregation tendency of MWCNT in nanocomposites and significantly improves processability. Polythiophene-functionalized multiwalled carbon nanotube (PTCNT-COOH) binary nanocomposites were used to prepare ternary silver nanocatalyst (TNC) which contains conducting polythiophene layer. The forces of attraction between functionalized multiwalled carbon nanotube and polythiophene were predominantly non-covalent attractive forces such as π-interaction, hydrogen bonding and van der Waals forces. Silver nanoparticles were directly attached to the functionalized multiwalled carbon nanotubes (MWCNT-COOH) in binary silver nanocatalysts (BNC). The preparation, properties, and characterization of PTCNT-COOH 300 Ag (TNC) and MWCNT-COOH Ag (BNC) have been discussed in chapter 4.[57]

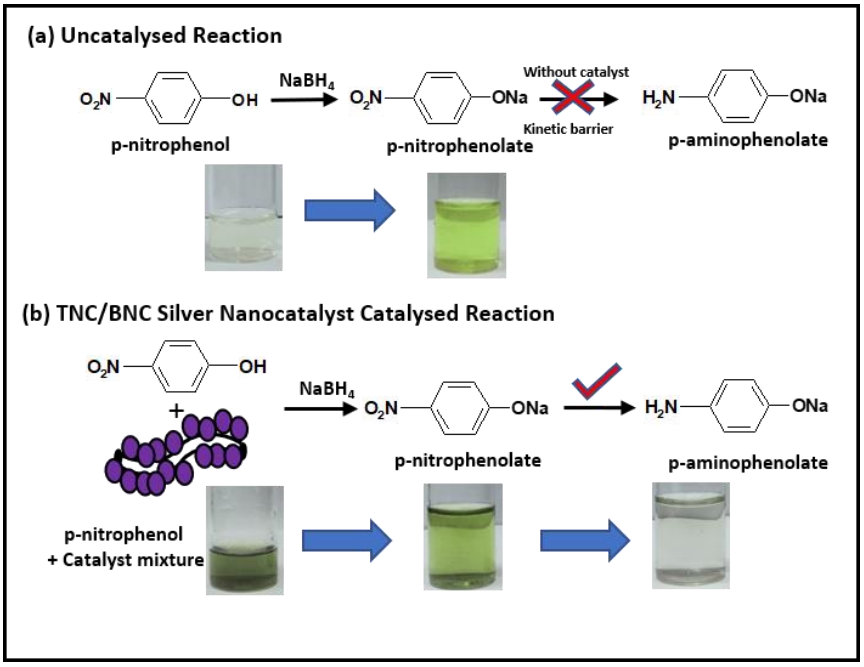

Figure 5.4. *Schematic representation of (a) reactions of p-nitrophenol with $NaBH_4$ and (b) silver nanocatalysts (BNC/TNC) catalyzed reaction of p-nitrophenol using $NaBH_4$.*

Table 5.1. *Name of nanocatalyst, initial concentrations of P-NP, $NaBH_4$, nanocatalyst, final concentrations of P-NP, $NaBH_4$, nanocatalysts, solvents, rate constant (k), and the activity factor.*

Sl. No.	Catalyst[a]	Initial concentrations of reaction mixtures			Final concentration of reaction mixture			Solvent	k[b] (s^{-1})	Activity factor[c] (s^{-1} g^{-1})
		P-NP in 2 mL (mM)	$NaBH_4$ in 2 mL (M)	TNC/ BNC (mg/mL)	P-NP in 4 mL (mM)	$NaBH_4$ in 4 mL (M)	BNC/ TNC (mg/ mL)			
1	TNC-0.02	0.01	0.10	0.02	0.005	0.05	0.01	water	$1.40x10^{-3}$	35.00
2	TNC-0.03	0.01	0.10	0.03	0.005	0.05	0.015	10% glycerol + water	-	-
3	TNC-0.04	0.01	0.10	0.04	0.005	0.05	0.02	water	$4.90x10^{-3}$	61.25
4	TNC-0.06	0.01	0.10	0.06	0.005	0.05	0.03	water	$1.34x10^{-3}$	113.34
5	TNC-0.10	0.01	0.10	0.10	0.005	0.05	0.05	water	$3.99x10^{-2}$	199.50
6	BNC-0.01	0.01	0.10	0.01	0.005	0.05	0.005	10% glycerol +water	$1.87x10^{-2}$	936.50
7	BNC-0.02	0.01	0.10	0.02	0.005	0.05	0.01	water	$1.10x10^{-3}$	27.50
8	BNC-0.03	0.01	0.10	0.03	0.005	0.05	0.015	10% glycerol+ water	-	-
9	BNC-0.04	0.01	0.10	0.04	0.005	0.05	0.02	water	$1.59x10^{-2}$	198.75
10	BNC-0.06	0.01	0.10	0.06	0.005	0.05	0.03	water	$3.64x10^{-2}$	303.34
11	BNC-0.10	0.01	0.10	0.10	0.005	0.05	0.05	water	$5.40x10^{-2}$	270.00

[a] Ternary nanocatalyst (TNC) or binary nanocatalyst (BNC) taken in different concentrations. [b] The rate constant obtained from the time dependent UV-vis studies. [b] The ratio rate constant divided by the weight of the catalyst used.

Heterogeneous ternary and binary nanocatalysts were utilized to convert p-nitrophenol to p-aminophenol in an aqueous medium. Due to the kinetic energy barrier, the reduction of nitrophenols to aminophenols did not proceed without a catalyst. Therefore, adding sodium borohydride to p-nitrophenol produces a greenish-yellow solution of p-nitrophenolate ion (see Figure 5.4.).[58] On the other hand, in the presence of ternary or binary nanocatalysts, colourless p-aminophenolate ions were formed from the greenish-yellow coloured p-nitrophenolate ion. The sonication process helps to adsorb the p-nitrophenol to the active sites of nanocatalysts.[59]

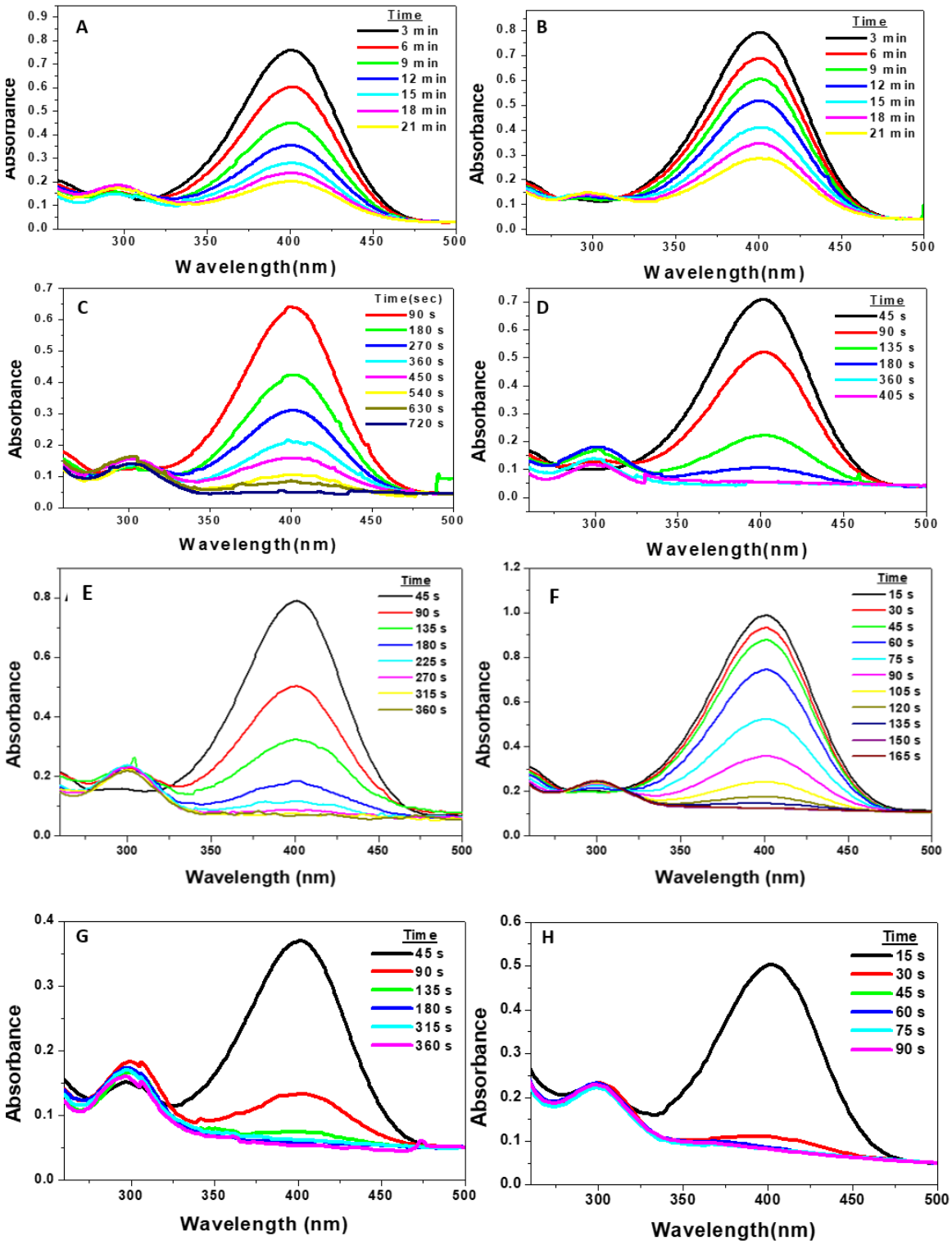

Figure 5.5. *UV-vis absorption spectra for reduction of p-nitrophenol using catalyst TNC-0.02 (A), BNC-0.02 (B), TNC-0.04 (C), BNC-0.04 (D) TNC-0.06 (E), BNC-0.06 (F), TNC-0.10 (G)and BNC-0.10 (H) in consecutive time intervals.*

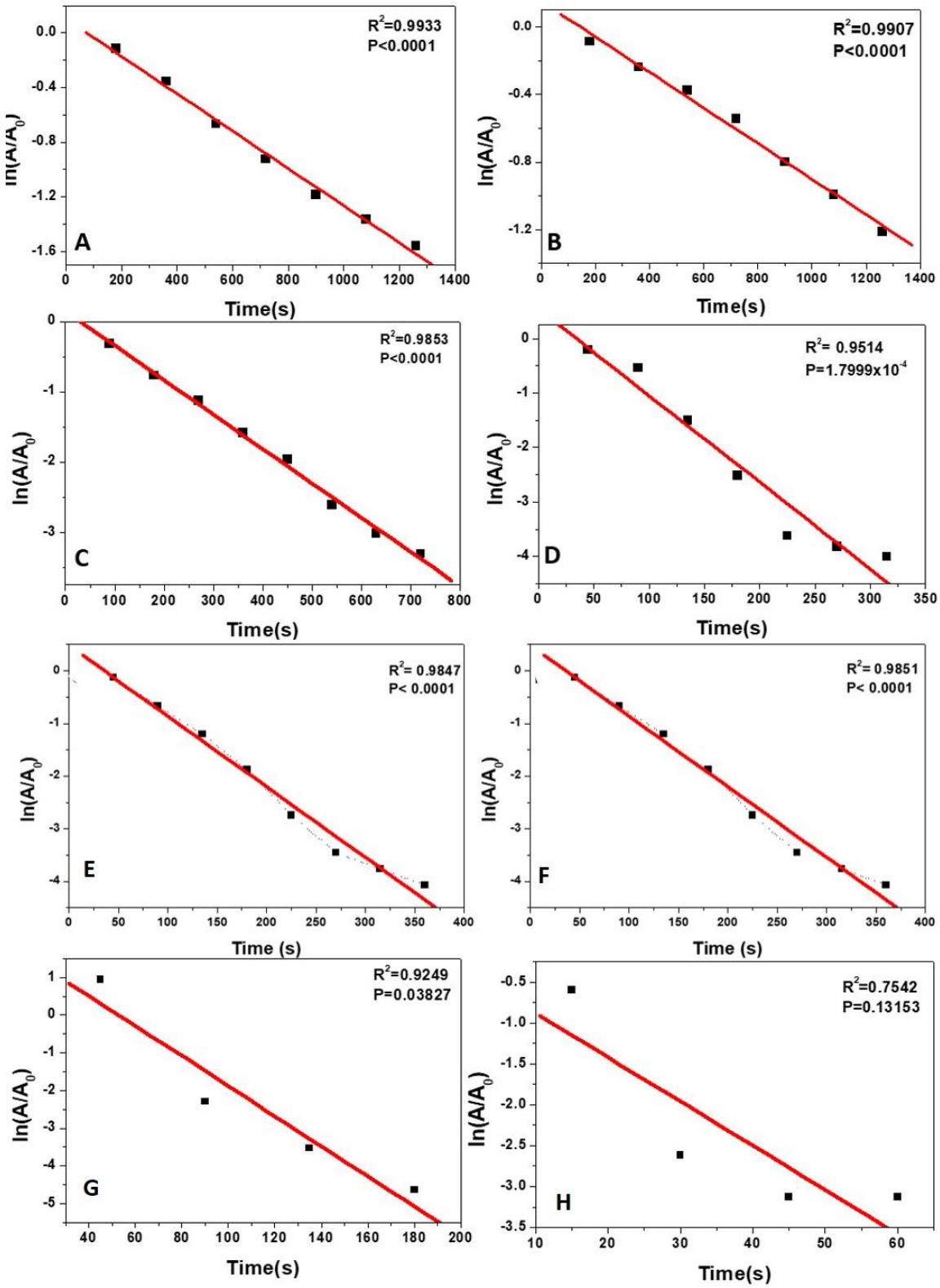

***Figure* 5.6.** *Linear relationship plot of ln (A/A$_0$) against time for p-nitrophenol reduction using TNC-0.02 (A), BNC-0.02 (B), TNC-0.04 (C), BNC-0.04 (D) TNC-0.06 (E), BNC-0.06 (F), TNC-0.10 (G)and BNC-0.10 (H)*

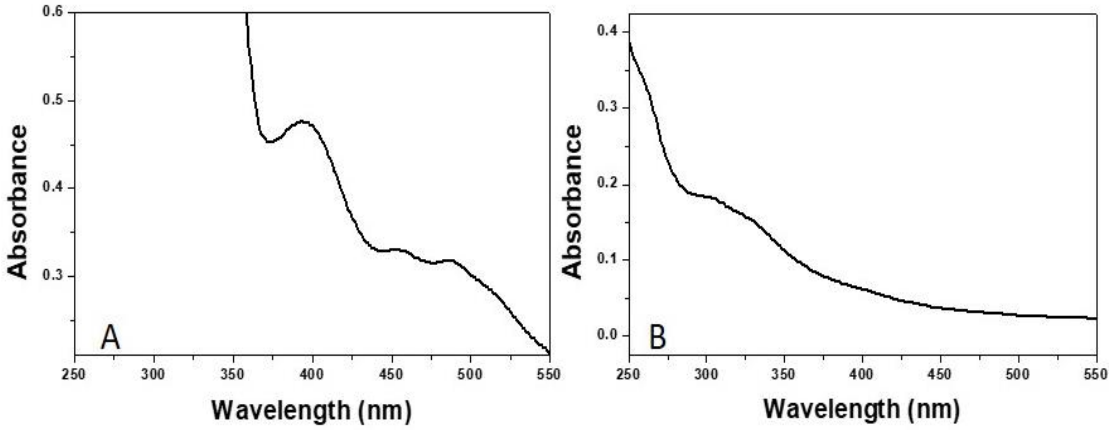

Figure 5.7. *UV-vis absorption spectra of silver nano colloids after one day of synthesis(A) and silver nano colloids after 7 days of synthesis(B).*

The catalytic conversion of p-nitrophenol to p-aminophenol was monitored by UV-vis absorbance spectroscopy by noting the decrease in p-nitrophenolate ion peak at 400 nm in successive time intervals after the start of the reaction. Silver nanocatalysts were named TNC-0.02, BNC-0.02, TNC-0.04, BNC-0.04, TNC-0.06, BNC-0.06, TNC-0.10, and BNC-0.10, in which digits represent the concentration of ternary or binary nanocatalysts in mg/mL initially taken in aqueous P-NP solution for catalytic studies (see **Table 5.1.**)**.** The p-nitrophenolate ion peak at 400 nm was produced immediately by adding sodium borohydride solution. As time progresses, the p-nitrophenolate ion peak intensity decreases with a concomitant increase of the new peak at 298 nm, corresponding to the p-aminophenolate ion (see **Figure 5.2.**).[58] The complete suppression of the peak at 400 nm indicated the reaction completion. Time-dependent UV-vis absorption spectra of nanocatalyst concentration TNC-0.02, BNC-0.02, TNC-0.04, BNC-0.04, TNC-0.06, BNC-0.06, TNC-0.10, and BNC-0.10 were recorded (see **Figure 5.5.**). The rate constants for this catalytically driven reaction were obtained by plotting ln (A/A_0) against time (see **Figure 5.6.**). The reaction follows pseudo-first-order kinetics; therefore, the rate constant can be obtained from the line's slope from linear regression fit.[60,61] The resultant rate constants were 0.0014 s^{-1}, 0.0011 s^{-1}, 0.0049 s^{-1}, 0.0159 s^{-1}, 0.0134 s^{-1}, 0.0364 s^{-1}, 0.0399 s^{-1} and 0.0540 s^{-1} respectively for the catalytic concentrations TNC-0.02, BNC-0.02, TNC-0.04, BNC-0.04, TNC-0.06, BNC-0.06, TNC-0.10 and BNC-0.10. Activity factor (the ratio of rate constant to the weight of catalyst used) were also calculated as 35.00 s^{-1} g^{-1}, 27.50 s^{-1} g^{-1}, 61.25 s^{-1} g^{-1}, 198.75 s^{-1} g^{-1}, 113.34 s^{-1} g^{-1}, 303.34 s^{-1} g^{-1}, 199.50 s^{-1} g^{-1} and 270.00 s^{-1}

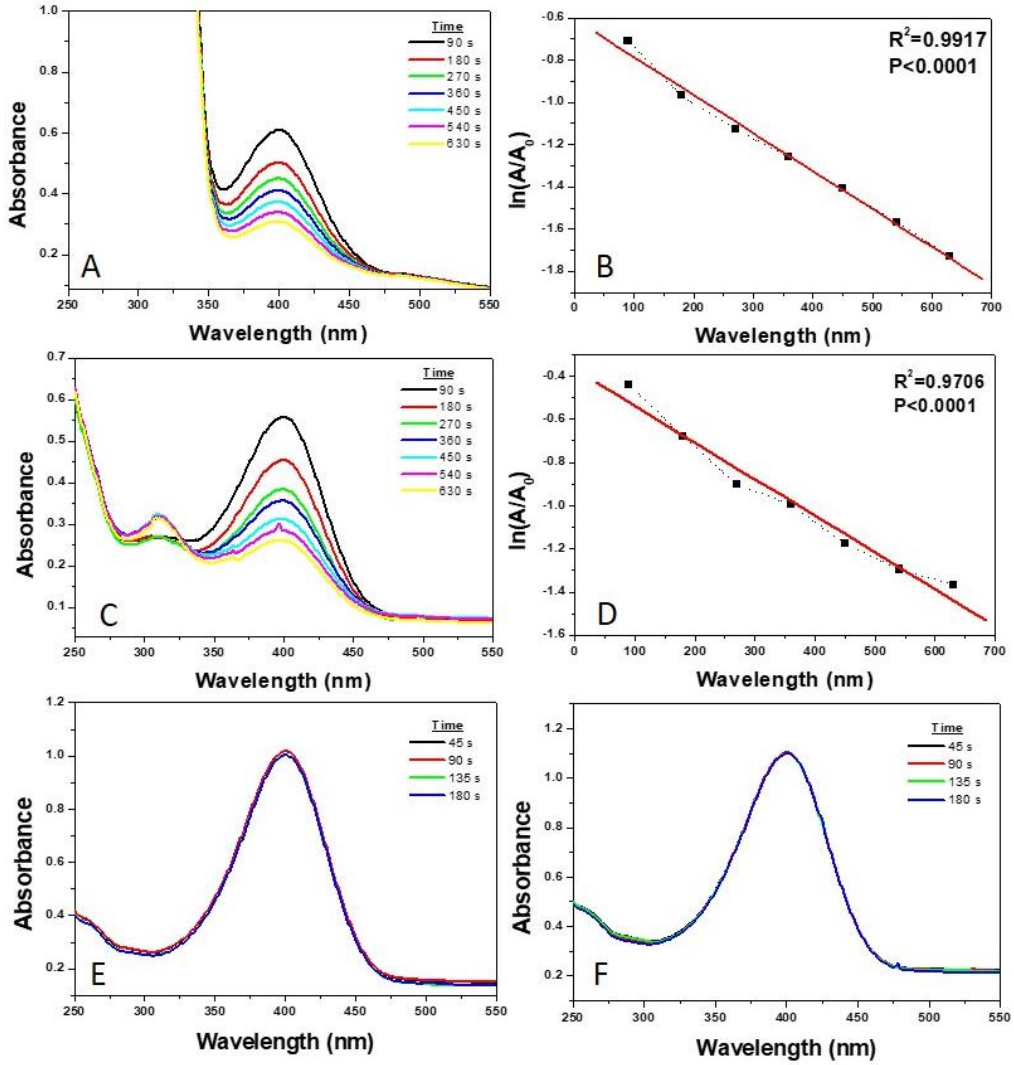

Figure 5.8. *UV-vis absorption spectra of reduction of p-nitrophenol using $NaBH_4$ using homogeneous colloidal silver nanoparticles as catalyst (A) and its linear relationship plot of ln(A/A_0) against time on first day after the synthesis of silver nano colloid (B). UV-vis absorption spectra of reduction of p-nitrophenol using $NaBH_4$ using homogeneous colloidal silver nanoparticles catalyst (C) and its linear relationship plot of ln(A/A_0) (D) against time on seventh day after the synthesis of silver nanocolloid. UV-vis absorption spectra of reduction of p-nitrophenol using $NaBH_4$ using PTCNT-COOH 300 as catalyst (E) and reduction of p-nitrophenol using $NaBH_4$ using MWCNT-COOH as catalyst (F).*

g^{-1} for TNC-0.02, BNC-0.02, TNC-0.04, BNC-0.04, TNC-0.06, BNC-0.06, TNC-0.10 and BNC-0.10 respectively (see **Table 5.1.**). Rate constants of TNC-0.02 and BNC-0.02 are almost equal, but as nanocatalysts' concentration increases, approximately 2 to 3 times greater catalytic activity was obtained for BNC rather than TNC. Silver nanoparticles

decorated TNC, and BNC nanocatalysts relay on electrons flow from $NaBH_4$ to p-nitrophenol (P-NP) through silver nanoparticles for catalytic reduction. The slow kinetics of TNC compared with BNC could be attributed to the electrical movement of electrons into conducting polythiophene layer.[57,62] Control experiments conducted using silver nanoparticles (Ag NPs) have shown characteristic surface plasmon resonance peaks at 400 nm in freshly prepared conditions (see **Figure 5.7. A**). The rate constant for p-nitrophenol reduction using Ag NPs (~ 0.03 mg/mL final concentration) was found ($k = 1.82 \times 10^{-3}\ s^{-1}$) to be approximately in the same range that obtained for TNC-0.02 and BNC-0.02 (see **Figure 5.8. A** and **B**). In colloidal silver nanoparticles, the surface plasmon resonance peak was overlapped with the nitrophenolate ion peak, making it difficult to note the reaction completion (see **Figure 5.8. A**). The reduction reaction carried out after the ageing of Ag NPs solution for seven days has shown a slight decrease in the rate constant and settling of nano colloidal silver nanoparticles (see **Figure 5.8. C**). Besides, the UV-vis absorption spectra of colloidal silver nanoparticles taken after seven days do not possess surface plasmon resonance peaks (**see Figure 5.7. B**). Although colloidal silver nanoparticles in freshly prepared conditions act as good catalysts, their aggregation tendency, stability, and recyclability were major issues. Control experiments conducted using MWCNT-COOH and PTCNT-COOH 300 without silver nanoparticles have not shown catalytic activity (see **Figure 5.8 E** and **F**). Functionalized multiwalled carbon nanotubes/polymer play a vital role as a heterogeneous framework to accommodate silver nanoparticles to prevent agglomeration, rapid oxidation, and leaching.

5.3.2. Optimization of nanocatalyst amount.

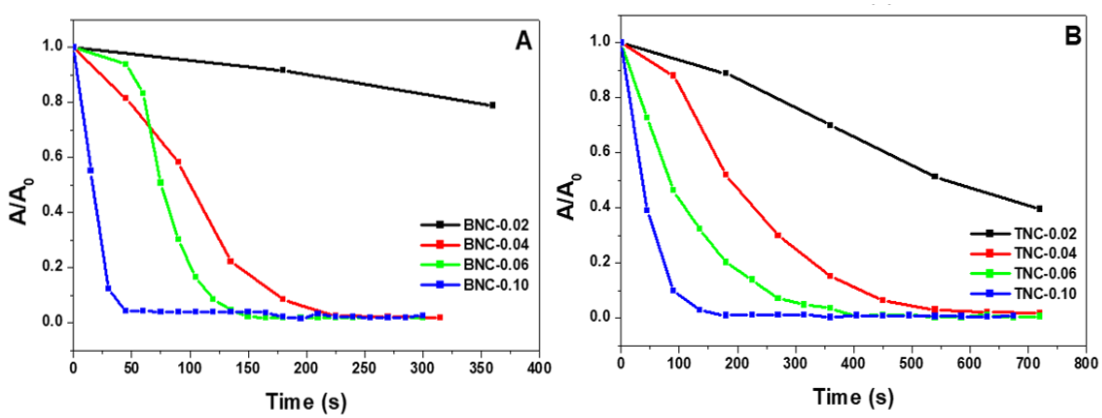

Figure 5.9. *Plot of (A/A_0) against time for TNC catalysed reactions (A) and BNC catalysed reactions (B) for different concentrations of catalyst 0.02 mg/mL, 0.04 mg/mL, 0.06 mg/mL, and 0.10 mg/mL taken in p-nitrophenol solution.*

Table 5.2. *Comparing catalysts, concentrations of reagents, rate constants, and activity factors obtained in the present study with recent other literature reports.*

Sl. No.	Catalyst	Catalyst Amount	p-aminophenol		$NaBH_4$		Rate constant (k)		Activity factor		Ref.
			Conc.	Vol. (mL)	Conc.	Vol. (mL)	s^{-1}	min^{-1}	$s^{-1} g^{-1}$	$min^{-1} g^{-1}$	
1	Ag NPs −PANI/ MWCNT	1.00 mg	0.10 mM	0.2 mL	0.1 M	2 mL	0.0054	-	5.40	-	(1)
2	Ag@MWCNTs-polymer	10 mg	0.10 mM	15 mL	5 mM	15 mL	0.0079	-	11.64	-	(2)
3	NiS-$NiCo_2O_4$ @C	0.017 mg/mL	0.1 mM	3 mL	0.08 M	-	-	1.78	-	-	(3)
4	Ag CD-MA@Fe MNps (AgNC)	5 mg	0.12 mM	1.5 mL	12 mM	1.5 mL	-	0.674	-	-	(4)
5	Pd@PUN	30 mg	0.10 mM	20 mL	40 mM	10 mL	-	4.96	-	-	(5)
6	Ag@PDA@poly(M-POSS)	0.005 mg/mL	20 mM	50µL	0.2 M	20 mL	-	0.837	-	1.67×10^5	(6)
7	PSMAA/ Ag	2 mg	0.1 mM	2 mL	60 mM	0.5 mL	0.0082	-	-	-	(7)
8	Fe_3O_4-CS-Ag NPs	2 mg/mL	0.125 mM	2 mL	0.5 M	0.1 mL	-	0.56	-	-	(8)
9	TNC-0.06	0.06 mg/mL	0.01 mM	2 mL	0.1 M	2 mL	0.0134	0.804	113.34	6.8×10^3	**Present work**
10	BNC-0.06	0.06 mg/mL	0.01 mM	2 mL	0.1 M	2 mL	0.0364	2.184	303.34	1.8×10^4	

The optimum nanocatalyst concentrations of TNC and BNC for reducing p-nitrophenol (1.0×10^{-4} M) were selected by plotting A/A_0 against time for different catalyst concentrations (see **Figure 5.9.**). The optimum nanocatalyst concentration has been selected based on the minimum quantity of a nanocatalyst needed to catalyze reaction at a measurable speed. In general, for all catalyst concentrations, as the time increases, the A/A_0 value decreases and reaches a steady minimum in the curve, corresponding to the completion of the reaction. The time required to reach a steady minimum for TNC-0.04, TNC-0.06, and TNC-0.10 were 550 s, 315 s, and 150 s, and that for BNC-0.04, BNC-0.06 and BNC-0.10 were 225 s, 150 s, and 50 s respectively. Therefore, even though TNC-0.10 and BNC-0.10 have given faster reaction kinetics than TNC-0.06 and BNC-0.06, the latter was selected as optimum catalyst concentration due to lower catalyst concentration and

measurable speed. By considering other literature works reported recently on p-nitrophenol reduction using different metal incorporated nanocomposites, one of the leading catalytic activities observed in both BNC and TNC catalyzed reduction (see **Table 5.2.** for comparison with other reports).

5.3.3. Recycling studies.

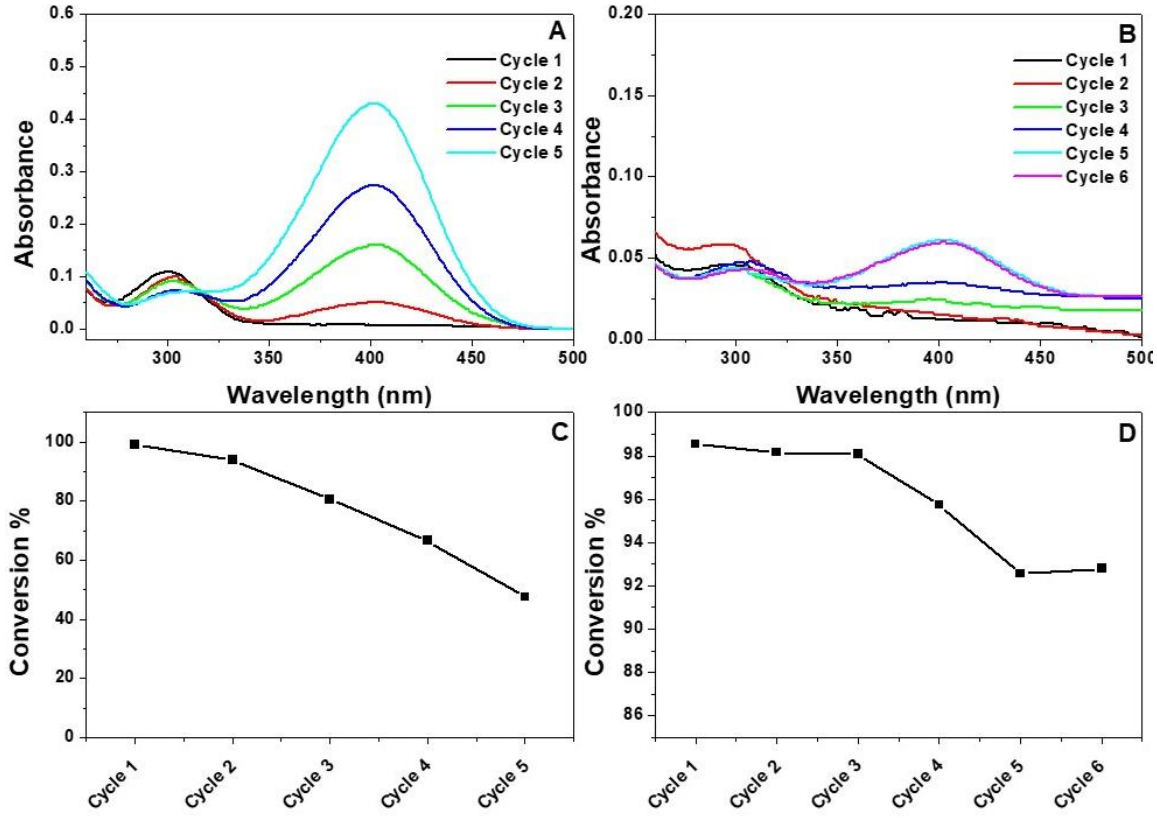

Figure 5.10. *UV-vis absorption spectra of TNC 0.06 catalysed (A) and BNC-0.06 catalysed reaction (B) for successive catalytic cycles. Catalytic conversion percentage of TNC-0.06 (C) and BNC-0.06 (D) in successive catalytic cycles.*

The recycling studies of the nanocatalysts TNC and BNC were carried out, and catalytic efficiency in the recycling process was recorded via UV-vis absorption spectra (see **Figure 5.10.**). TNC was recycled and analyzed for five consecutive cycles and BNC for six consecutive cycles by fixing the reaction time as 10 min for each cycle. Here catalyst was recovered by centrifugation and reused for the next catalytic cycle after washing with water. The catalytic conversion (%) of p-nitrophenol to p-aminophenol has been determined using the equation,

$$\boldsymbol{Conversion}\ (\%) = \left(\mathbf{1} - \frac{\boldsymbol{A}}{\boldsymbol{A_0}}\right)\mathbf{x\ 100}$$

Where A_0 and A are the absorption maxima of the p-nitrophenolate ion at the initial time (t_0) and monitoring time (t), respectively. Catalytic conversion (%) for successive cycles indicated better BNC efficiency than TNC for six catalytical cycles (see **Figure 5.10. C** and **D**). TNC has shown catalytic conversion of 47.56 % in the 5th catalytic cycle, whereas BNC has shown 92.80 % conversion in the 6th cycle in identical conditions. The conversion (%) obtained from the UV-vis absorbance spectroscopy have revealed that nanocatalyst BNC activates the reaction more than TNC in multiple cycles. Nanocatalysts recovered from the reaction mixture via centrifugation and washing before subsequent uses. TNC being better dispersive than BNC via sonication, have more leaching effect of silver than the latter case.

5.3.4. Elemental composition and morphology of recycled nanocatalysts.

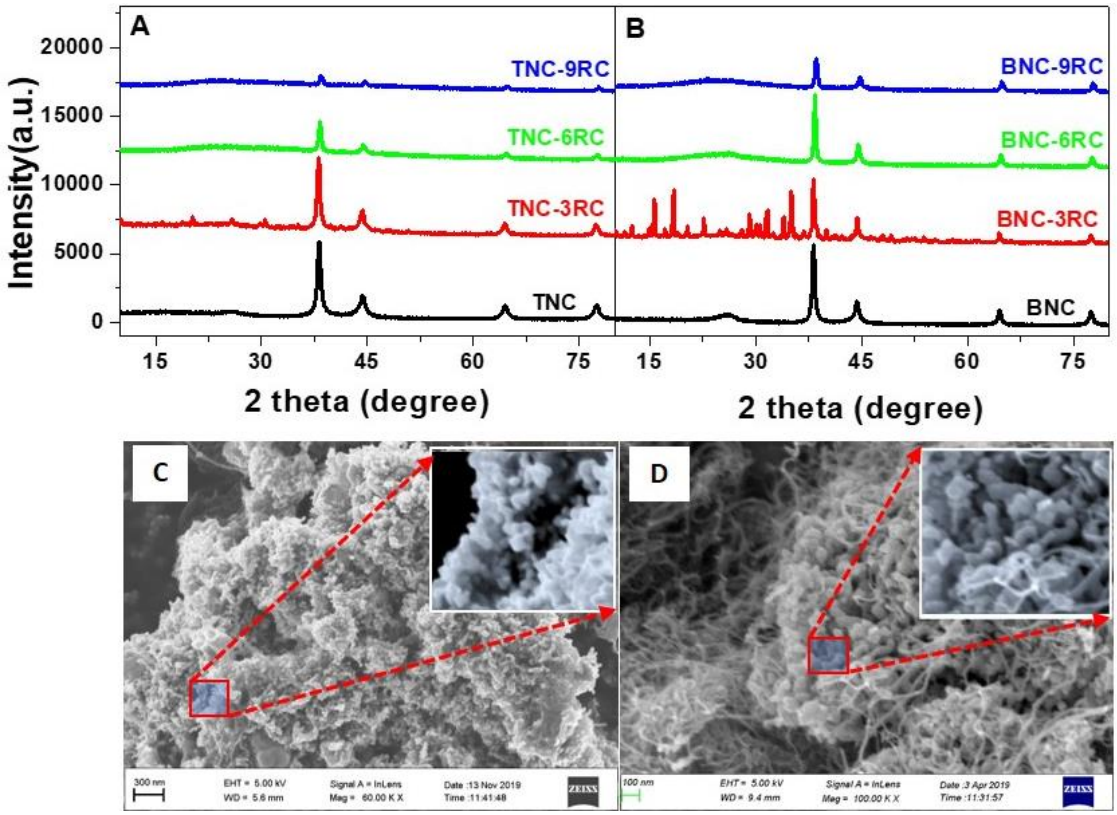

Figure 5.11. *X-ray diffraction patterns of TNC and recycled TNCs (A), BNC and recycled BNCs (B) after 3rd, 6th and 9th catalytic cycles. FE-SEM images of TNC (C) and BNC (D) as pristine nanocatalyst (enlarged portion is shown in inset).*

We have subjected the recycled catalysts to powder X-ray diffraction studies to trace changes during the recycling (see **Figure 5.11. A** and **5.11. B**). TNC and BNC obtained after the third, sixth, and ninth cycles were named TNC-3RC, TNC-6RC, TNC-

9RC, BNC-3RC, BNC-6RC, BNC-9RC; the figure represents the recycle number. Comparison of powder X-ray diffraction patterns of pristine catalysts with recycled catalysts revealed that intensity of crystalline diffraction peaks corresponding to silver nanoparticles at 2θ values 38.15°, 44.33°, 64.52°and 77.46° were decreased considerably after the 6th catalytic cycle (see **Figure 5.11. A** and **5.11. B**).[45] A substantial decrease in intensity of diffraction peaks of silver nanoparticles was noticeable on the 9th catalytic cycle of TNC than BNC. The more decrease in TNC nanocatalyst intensity than the BNC nanocatalyst in higher catalytic cycles was due to the loss of a higher amount of silver nanoparticles during separation, washing, and sonication. The diffraction pattern of BNC-3RC has given crystalline peaks other than silver nanoparticles matching with the crystalline form of sodium metaborate formed as a by-product from sodium borohydride (see **Figure 5.12.**).[24,63-65] The inner core structure of the recycled nanocatalysts TNC-3RC and BNC-3RC were determined using X-ray photoelectron spectroscopy (see **Table 5.12.**). Functionalized multiwalled carbon nanotubes contain 94.42 atomic percent of C 1s and 5.58 atomic percent of O 2s.[57] Recycled binary nanocatalyst BNC-3RC have shown characteristic peaks of C 1s (284.77 eV), O 1s (532.47 eV), Na 1s (1072.27 eV), Ag 3d (374.44 eV) and B 1s (192.77 eV) with atomic percentage of 91.0%, 6.6 %, 1.3 %, 0.8 % and 0.2% respectively. On the other hand, TNC-3RC have shown characteristic peaks of C

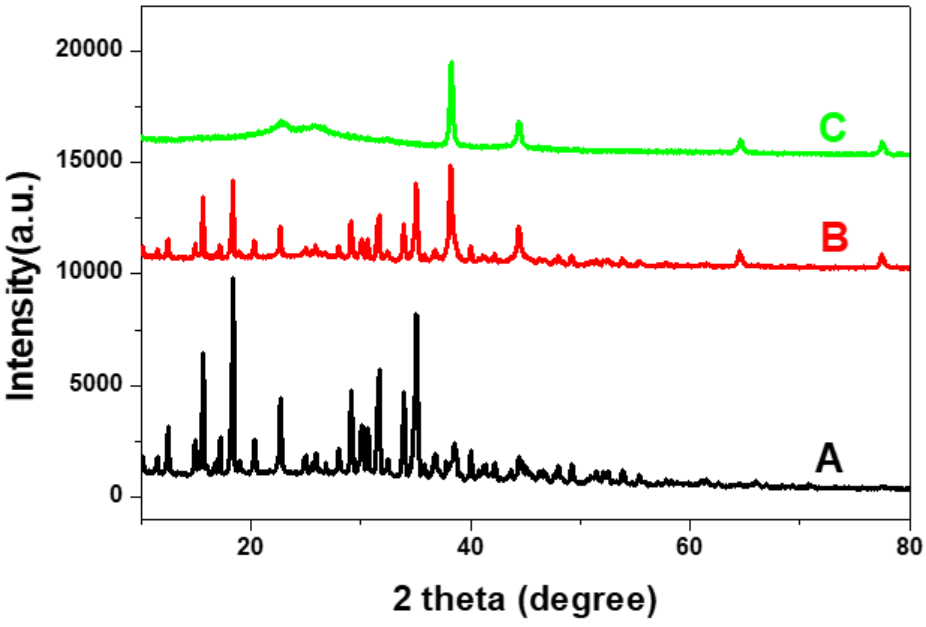

Figure 5.12. *WXRD patterns of (A) byproduct separated from the reaction residue, (B) BNC-3RC and (C) BNC-3RC after repeated centrifugation and washing.*

1s (284.78 eV), O 1s (532.18 eV), Na 1s (1074.08 eV), Ag 4s (102.11 eV), B 1s (192.77 eV) and S 2p (166.47 eV) with atomic percentage 76.9 %, 21.9 %, 0.3 %, 0.5 %, 0.2 % and 0.1 % respectively. The higher atomic percentage of C1s in BNC-3RC (91.0 %) than TNC-3RC (76.9 %) was mainly due to the binary components, which consists of functionalized multiwalled carbon nanotubes and silver nanoparticles only. The presence of sodium metaborate hydrates as a by-product, intermediate layer of conducting polythiophene, and dopants influence the total atomic percent of TNC (see **Figure 5.13.**). The atomic composition of silver atoms of BNC-3RC was higher than TNC-3RC, which matches with powder x-ray diffraction data. The decrease in the atomic percentage of silver could be due to the separation of silver nanoparticles in the recycling process.

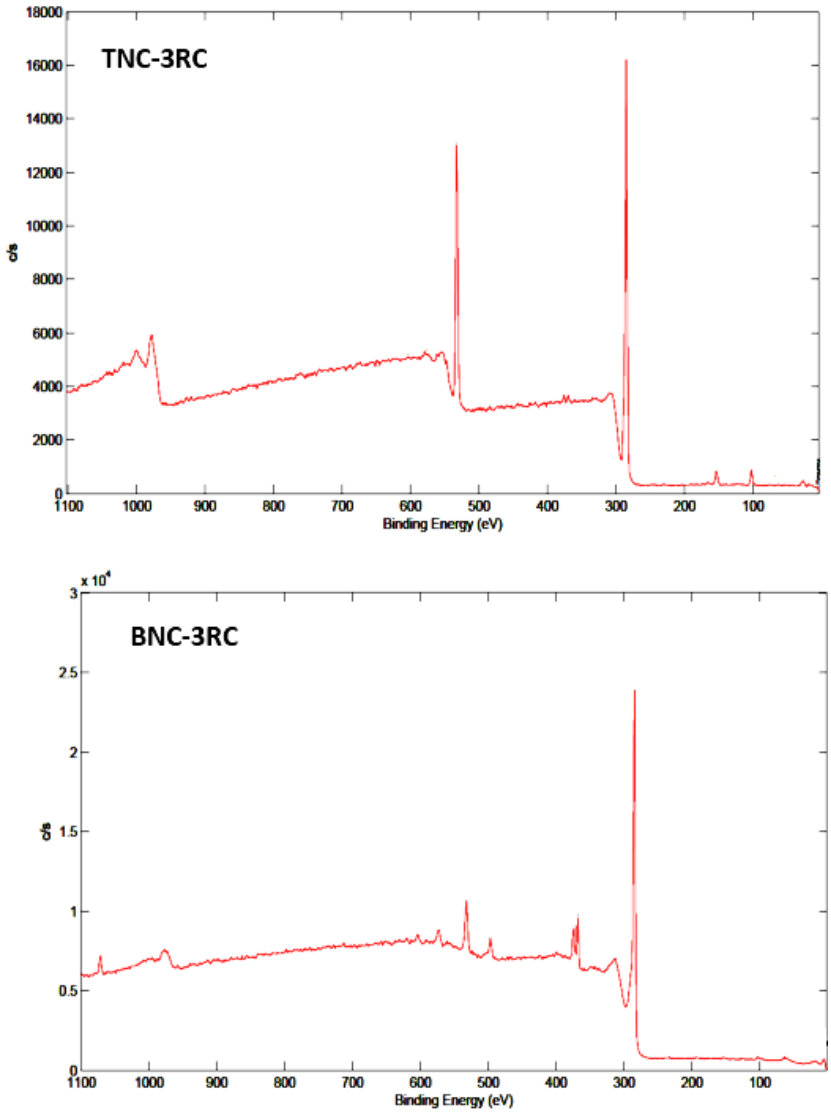

Figure 5.13. XPS spectra of TNC-3RC and BNC-3RC.

Silver nanoparticles embedded pristine TNC and BNC nanocatalysts were subjected to field emission scanning electron microscopy. TNC contains silver nanoparticles with an average size of 25 ±5 nm, which exists in a tangled manner on the PTCNT-COOH 300 framework, whereas BNC contains nanoparticles with an average size of 45 ± 5 nm supported on MWCNT-COOH (see **Figure 5.11. C** and **D** for FESEM images of TNC and BNC before catalytic use). The surface morphology and elemental distribution of the recycled catalyst surface have been traced by scanning electron microscopy and energy dispersive X-ray (EDX) analysis (see **Figure 5.14. C, D, E** and **F**). FE-SEM images of recycled nanocatalysts TNC-3RC and BNC-3RC have shown hexagonal crystalline faces over the nanocatalysts (**Figure 5.14. A** and **5.14. B**). The EDX elemental dot mapping showed a sodium atom percentage of 11.84 % on the TNC surface and 14.18 % on the BNC surface. The presence of sodium atoms and higher oxygen mass percentage from dot mapping images indicated the formation of sodium metaborate hydrates deposited in the hexagonal phase over the nanocatalyst surface. The recycled nanocatalyst TNC-3RC and BNC-3RC contain 1.61 and 1.00 atomic percent of silver atoms within the EDX analysis limitations (see **Table 5.3.**). A mechanistic view of recycled nanocatalyst (TNC or BNC) represented after catalytic hydrogenation of p-nitrophenol using sodium borohydride (shown in **Figure 5.14. G**). TNC and BNC could be reused for many cycles; however, the metaborates trapped in nanocatalysts could mask the catalytic activity.

Table 5.3. *The atomic percentage of C, O, Na, B, Ag, and S in TNC-3RC and BNC-3RC.*

Element	**From XPS analysis[a]**	
	TNC-3RC (atom %)	**BNC-3RC (atom %)**
C	76.9	91.0
O	21.9	6.6
Na	0.3	1.3
B	0.2	0.2
Ag	0.5	0.8
S	0.1	-

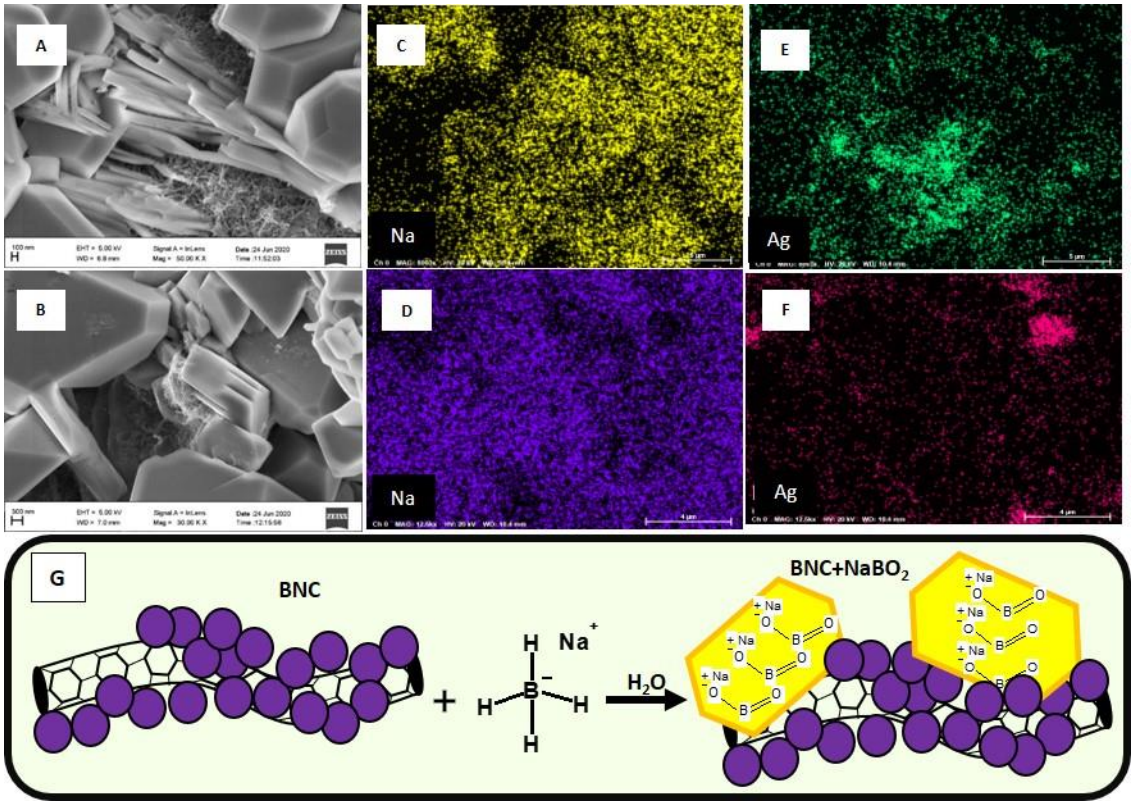

Figure 5.14*. FE-SEM images of TNC-3RC (A) and BNC-3RC (B), EDX colour mapping of sodium in TNC-3RC (C), sodium in BNC-3RC (D), silver in TNC-3RC (E) and silver in BNC-3RC (F). Schematic representation of the existence of metaborate by-product over a recycled catalyst (G).*

5.3.5. Optimization of solvent-water mixture for reduction.

The kinetic and mechanistic aspects of BNC and TNC catalyzed p-nitrophenol reduction were systematically studied using different solvent-water mixtures like glycerol-water, ethylene glycol-water, ethanol-water, and 1,4-dioxane-water. The different catalyst concentrations like TNC-0.03, BNC-0.03, TNC-0.06, and BNC-0.06 were used to reduce p-nitrophenol (1.0×10^{-4} M, 5 mL) by the addition of $NaBH_4$ (1.0×10^{-1} M, 5 mL) in the presence of different volume % of solvent-water mixtures. The time of decolourization was noted as the time to complete the reaction. The reaction completion time versus different volume percentages of solvent-water mixtures (5 % v/v, 10 % v/v, 20 % v/v, 30 % v/v, 40 % v/v and 50 % v/v) were plotted (see **Figure 5.15.**). The reduction reaction has shown a faster reaction in glycerol-water, and ethylene glycol-water mixture, especially in the 5% - 30% percent volume, and after that, the reaction slows down as the medium's viscosity increases. In the ethanol-water mixture, the reaction rate was slower than in the above two mixtures and decolourization time increased as the volume percentage of ethanol increased.

The least reactivity was observed in 1,4-dioxane-water mixture, which could be easily understood from the non-availability of the active hydrogen in it. Therefore, the order of catalytic reactivity obtained in different solvent-water mixtures was glycerol-water > ethylene glycol-water > ethanol-water > 1,4-dioxane-water.

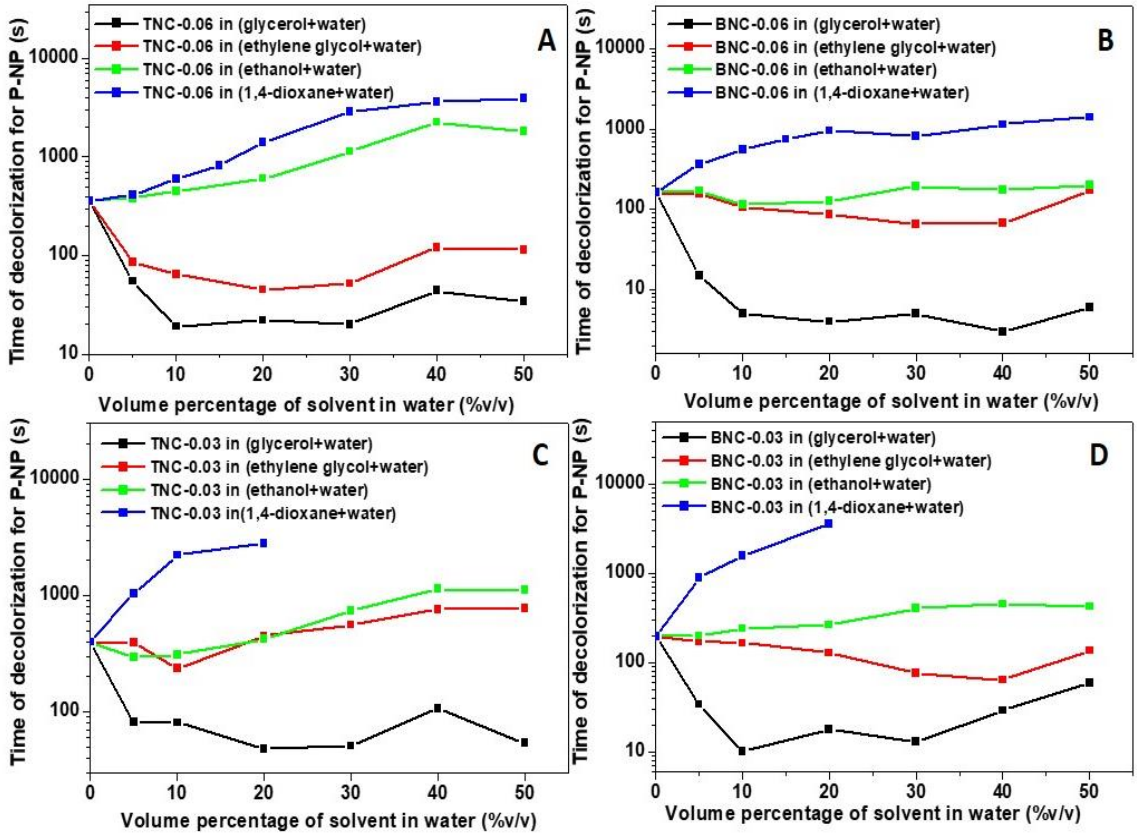

Figure 5.15. *Time of decolourization plotted against different volume percentage of solvent-water mixture using P-NP: $NaBH_4$ molar ratio 1:1000 with TNC-0.06, BNC-0.06, TNC-0.03 and BNC-0.03 catalysts.*

5.3.6. Optimization of [P-NP]: [$NaBH_4$] molar ratio.

Catalytic hydrogenation of p-nitrophenol was conducted by varying the molar ratio of [P-NP]: [$NaBH_4$] using TNC-0.06 and BNC-0.06 in a 10% v/v glycerol-water mixture. The [P-NP] to [$NaBH_4$] molar ratio has varied from 1:50, 1:100, 1:150, 1:250, 1:500 to 1:1000 in water and 10 % glycerol-water mixture by fixing the concentration of P-NP solution as 1×10^{-4} M. The decolourization time in catalytic reduction versus $NaBH_4$ to P-NP molar ratio was plotted (see **Figure 5.16. A**). The decolourization studies have revealed that reaction follows pseudo-first-order kinetics approximately at a mole ratio 500 in water, which was reduced to 250 in the glycerol-water mixture.[61] A major disadvantage of

reducing

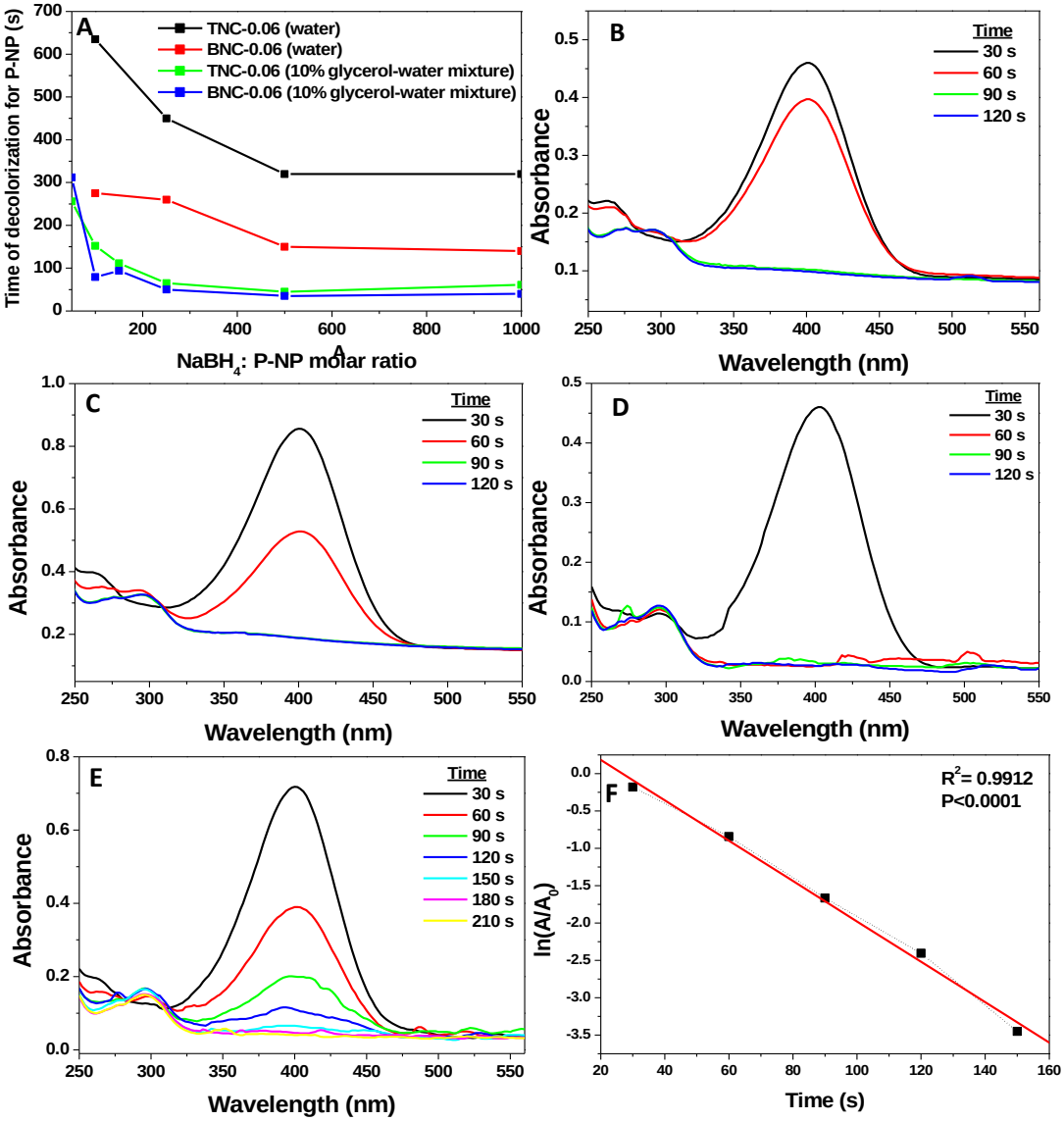

Figure 5.16. *Time of decolourization plotted against different $NaBH_4$ concentrations in water and 10% glycerol-water mixture using TNC-0.06 and BNC-0.06 catalysts (A). UV-vis absorption spectra of reduction of p-nitrophenol using catalyst TNC-0.06 [PNP: $NaBH_4$ molar ratio 1:100](B) using BNC-0.06 [PNP: $NaBH_4$ molar ratio 1:100] (C) and BNC-0.03 [PNP: $NaBH_4$ molar ratio 1:200] [D] in 10% glycerol-water solvent mixture. UV-vis absorption spectra of reduction of p-nitrophenol using catalyst BNC-0.01 [PNP: $NaBH_4$ molar ratio 1:200 (E) and linear relationship plot of $ln(A/A_0)$ against time for BNC-0.01 for PNP: $NaBH_4$ molar ratio 1:200 (F) in 10% glycerol-water solvent mixture.*

nitrophenols with sodium borohydride in water was the excess utilization of $NaBH_4$ to obtain a reasonable reaction rate. Therefore, minimizing the $NaBH_4$ for p-nitrophenol

reduction can ensure more economic gain to the synthetic strategy and reduced toxicity effects. The UV-vis absorption spectra were recorded to show the minimum utilization of catalyst with P-NP to $NaBH_4$ molar ratio 1:100 in 10% glycerol- water mixture TNC-0.06, BNC-0.06, BNC-0.03 catalyst concentrations were shown in Figure 5.16. B, C and D. In the presence of a 10% glycerol-water mixture, BNC-0.03 exhibited the same kinetics as BNC-0.06 in water with P-NP to $NaBH_4$ molar ratio 1:1000. More interestingly, the catalytic reduction of p-nitrophenol executed with a minimal concentration of BNC-0.01 catalyst and P-NP to $NaBH_4$ molar ratio of 1: 200, excellent activity factor of 936.5 $s^{-1}g^{-1}$ was obtained in a 10% glycerol-water solvent mixture (see **Figure 5.16. E** and **F**).

5.3.7. The proposed mechanism for catalytic reduction.

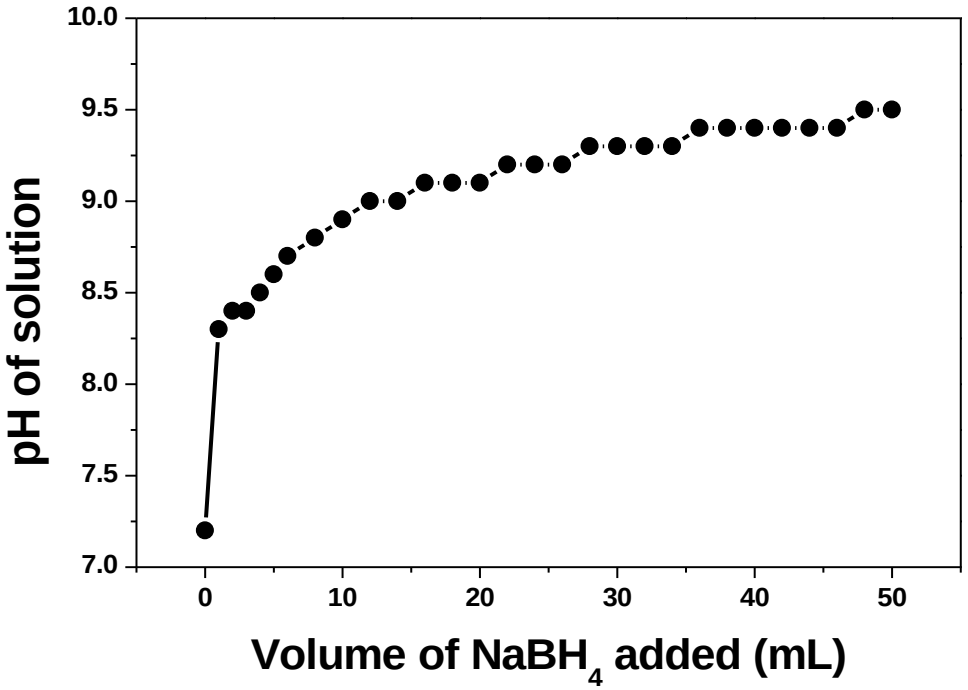

Figure 5.17. *Change in pH of glycerol-water mixture (20%) by the addition of $NaBH_4$.*

The catalytic reduction of p-nitrophenol using $NaBH_4$ as the reductant remains controversial. TNC and BNC catalytic performance in different solvent mixtures led us to gain some mechanistic evidence about the hydrogen source used to reduce p-nitrophenol. Many possible ways of reduction mechanisms were discussed in the literature.[39,43-48] It was already reported in the literature that the reduction of p-nitrophenol did not occur in nonpolar solvents.[39,43,44] But the involvement of protic solvents using $NaBH_4$ as a reducing agent for p-nitrophenol reduction is still inexplicit in its research. In the present experiment, it was noticeable that solvent mixtures like glycerol- water and ethylene glycol-water have

shown higher activity than water. Other solvent mixtures such as ethanol-water and 1,4-dioxane-water mixture have shown a slower reduction rate than water, giving prime evidence of active solvent hydrogen involvement in the nitro group's hydrogenation reaction. Sodium borohydride undergoes hydrolysis with water or solvolysis with other solvents containing active hydrogens and produces hydrogen gas.[66] Rate of hydrogen molecule production due to solvolysis in the investigated solvent-mixtures at 5% v/v - 30% v/v follow the order glycerol-water > ethylene glycol-water > water > ethanol-water > 1,4-dioxane-water. Three active hydrogens per molecule present in glycerol could be the reason for production of three hydrogen molecules by combining with hydride ions from sodium borohydride. Ethylene glycol has two active hydrogens; water and ethanol have one active hydrogen each, from which a corresponding number of hydrogen molecules could be produced by solvolysis. The ethanol-water mixture has comparably less capacity to form hydrogen molecules than water since $NaBH_4$ exhibited low solubility in ethanol than water. The 1,4-dioxane with hydrogens in closed chains was not active as other solvents. The 1,4-dioxane-water mixture, therefore, has minimal hydrogen production capacity. A direct influence was visible towards active hydrogens' contribution from different solvent molecules to reduce the nitro group. Neither the sodium borohydride nor the active hydrogen-bearing solvent molecules alone could directly ensure the nitrophenol hydrogenation completely. The active hydrogens in solvent molecules combine with the hydride ion from sodium borohydride to produce hydrogen molecules, making reduction reaction feasible. The pH of $NaBH_4$, glycerol, and glycerol-$NaBH_4$ mixture in water was checked using a pH meter. The pH of 20% glycerol was 7.2, and that of $NaBH_4$ solution ($1x10^{-1}$ M) was 10.3. The $NaBH_4$ solution ($1x10^{-1}$ M) was added to the glycerol (25 mL, 20%) solution, the pH of the corresponding solution mixtures was checked with the addition of 2 mL each. A graph was plotted with the volume of $NaBH_4$ solution added against the pH of the reaction mixture (see **Figure 5.17.**). The reaction mixture's pH increased by $NaBH_4$ addition and reached a pH of 9.5 by adding 50 mL 1×10^{-1} M $NaBH_4$ solution. The reduction mainly happened in alkaline conditions; therefore, the production of hydrogen molecules by the reaction of $NaBH_4$ with active solvent hydrogen was the major factor rather than the change in pH. The dielectric constant of solvent mixtures on the reduction rate was studied.[67-69] Solvent mixtures used in the present study have lower dielectric constants than water; however, reaction rates in the glycerol-water mixture and ethylene glycol-water mixture exhibited a higher reaction rate than in water. A plausible

mechanism has been shown in **Figure 5.18.** Two probable reasons could be attributed here for catalytical hydrogenation of nitro group by the silver nanocatalyst. Active hydrogen species could be produced via solvolysis of the glycerol-water mixture with sodium borohydride has the primary role in enhancing the catalytic reduction rate.[21,70,71] This reactive hydrogen species gets adsorbed on the catalyst's surface to convert p-nitrophenol to p-aminophenol.[21,72] Second possibility was the conventional way of catalytical hydrogenation by the hydrogen molecules produced in the solvolysis.[40,47] Faster kinetics of the p-nitrophenol reduction in glycerol-water mixture using $NaBH_4$ as reductant indicates that the major path could be highly energetically reactive hydrogen species involved in reduction.

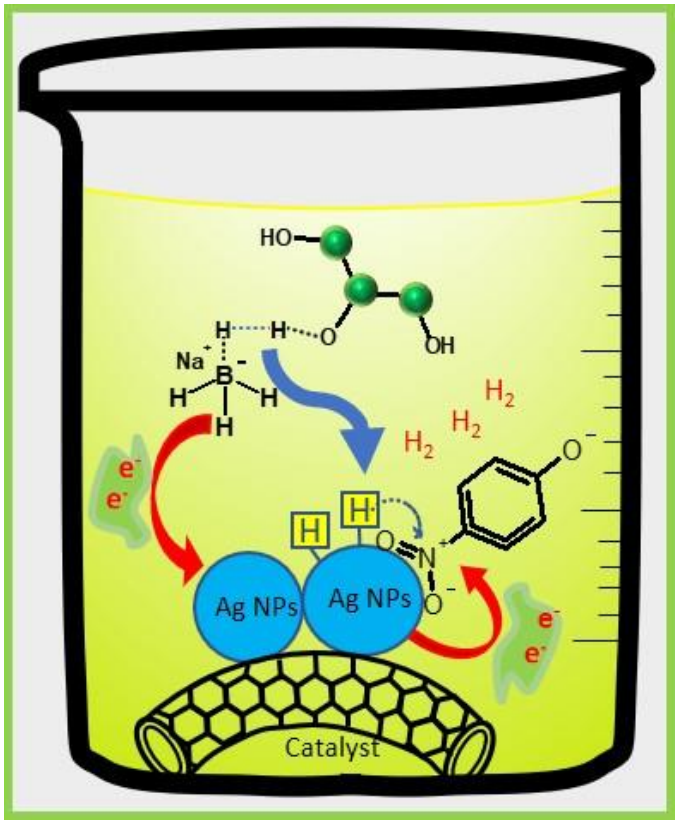

Figure 5.18. *Mechanism of active solvent enhanced green catalytic reduction of p-nitrophenol using $NaBH_4$ in 10% glycerol-water mixture.*

5.3.8. Relative yield and industrial-scale reduction of p-nitrophenol.

The relative yield of the p-aminophenolate ion was obtained from the calibration curve of known concentrations of p-aminophenolate (see **Figure 5.18.**). Different p-aminophenol solution concentrations were prepared from 5.0×10^{-4} M to 1.0×10^{-7} M. For

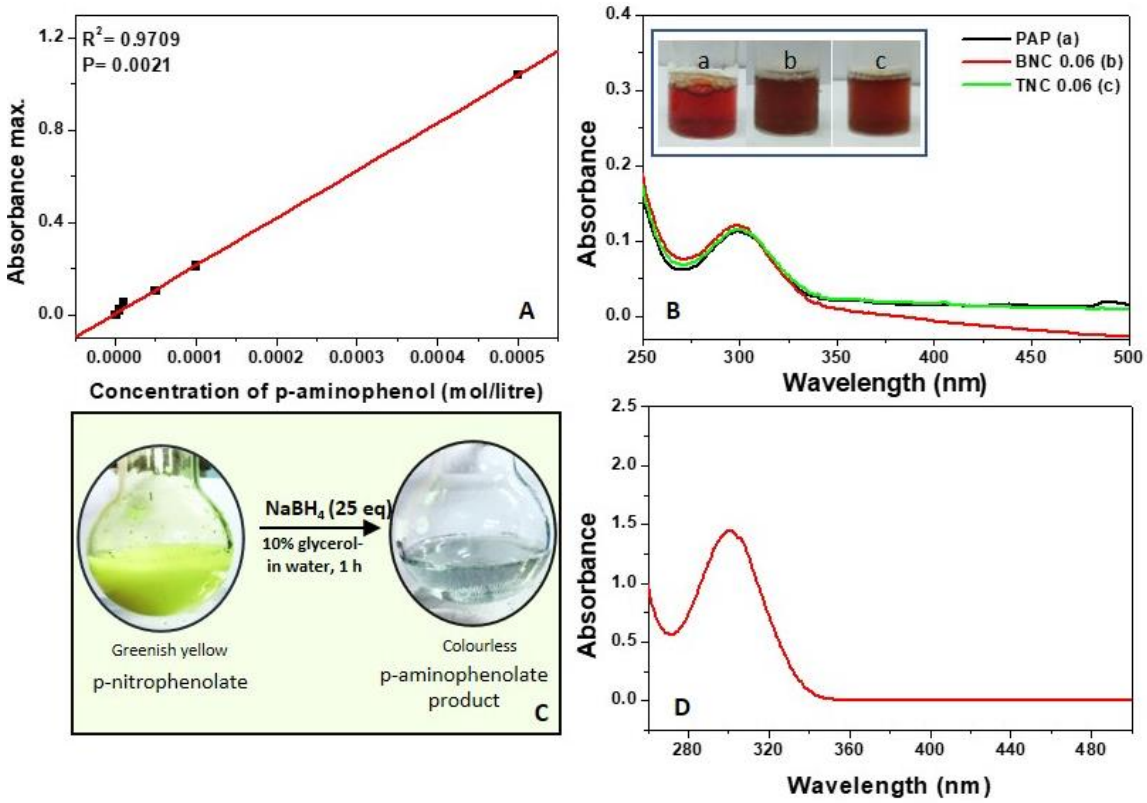

Figure 5.19. *Calibration plot of p-aminophenol in different concentrations (1 ×10^{-7} M to 5 ×10^{-4} M) (A), UV-vis absorption spectra of the standard solution of p-aminophenolate ion, p-aminophenolate obtained from catalytic reduction using TNC-0.06 and BNC-0.06 (in 1 ×10^{-4} M) (B), reduction of p-nitrophenol in concentrated solution (10 mL, 15 g/L) using P-NP: $NaBH_4$ molar ratio 1:25 and BNC-0.18 (0.18 mg/mL) in 10% glycerol-water mixture (C), and UV-vis spectrum p-aminophenolate produced by bulk concentration scale reduction (D).*

measuring the absorbance of the p-aminophenolate ion, a freshly prepared $NaBH_4$ solution (10 mL, 1.0 ×10^{-1} M) was added to each known concentration of p-aminophenol. The absorbance of p-aminophenolate ion obtained from nano catalytic reduction of p-nitrophenol (1.0 ×10^{-4} M) almost matched the known concentration of aminophenol, indicating complete conversion (see **Figure 5.19. B**). The synthetic utility of amino phenolate product has been substantiated by diazotization reaction (inset of **Figure 5.19. B**). Catalytical conversion of p-nitrophenol to p-aminophenol in 10% glycerol-water mixture using minimum P-NP to $NaBH_4$ molar ratio (1:25), by taking nanocatalyst concentration BNC-0.18 could be extended to high concentration scale up for industrial catalysis (near to the saturation limit of p-nitrophenol in water). The reaction completion was observed in green reaction conditions within one hour (see **Figure 5.19. C** for

photographs). The reaction mixture's UV-vis absorption spectra taken after one-hour reaction time have shown a peak at 298 nm corresponding to p-aminophenolate ion (see **Figure 5.19. D**). The absence of the p-nitrophenolate ion peak at 400 nm and the appearance of a single peak at 298 nm validated the complete reduction of p-nitrophenol to p-aminophenolate. Aminophenol's widespread applications in commercial and industrial fields demand bulk-scale hydrogenation of nitrophenol, which can be successfully prepared using heterogeneous silver nanocatalysts and by the utilization of a less volume percentage of glycerol.[73,74]

5.3.9. Antibacterial activity:

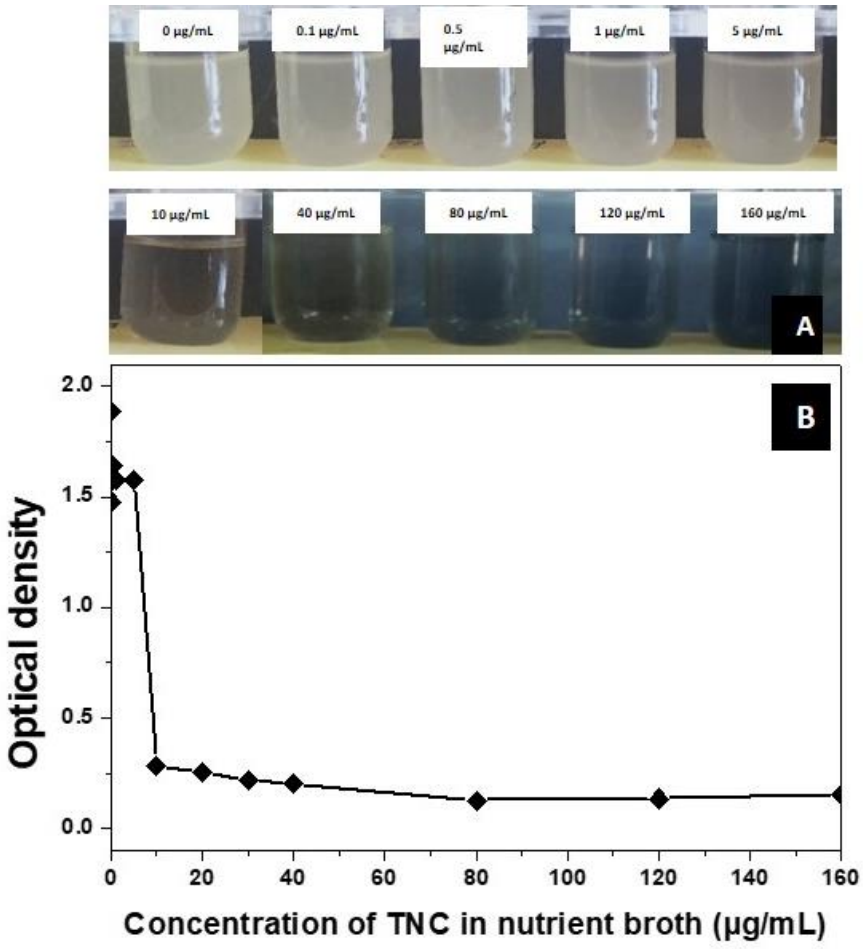

Figure 5.20. *Photographs of mixtures of E. coli bacteria culture with different concentrations of TNC taken after overnight incubation (A). The plot of optical density versus the concentration of TNC for the antibacterial study at 660 nm (B).*

Antibacterial activity studies of the nanocomposite TNC have been carried out on Escherichia coli, a frequently used model organism in life science research.[75,76] Silver nanoparticles act as good antibacterial agents depending on particle size and shape.[25,26] Ternary silver nanocatalysts (TNC) have been taken for antibacterial study in different doses due to their ability to maintain appreciable dispersion for longer. Antibacterial activity and minimum inhibitory concentration (MIC) of nanocomposite have been studied by the tube dilution method. Different concentrations of TNC such as 1 $\times 10^{-1}$ µg/mL, 5 $\times 10^{-1}$ µg/mL, 1 µg/mL, 5 µg/mL, 10 µg/mL, 20 µg/mL, 30 µg/mL, 40 µg/mL, 80 µg/mL, 120 µg/mL and 160 µg/mL were prepared. The mixtures were dispersed in a boiling tube for 10 min, and 50 µL actively growing E. coli culture was used as the inoculum for all tubes. It was incubated in a thermal shaker overnight at 37 ºC. Microbial growth in liquid medium was characterized by increased turbidity, for that incubation tubes were examined under bright light. The white turbidity resulting from *E. Coli* bacterial growth was almost absent in the medium above 10 µg/mL concentration of TNC (**Figure 5.20. A**). The result indicates that TNC exhibits good antibacterial activity against gram-negative *E. Coli* bacteria. Quantitative antibacterial activity was assessed by measuring optical density at 660 nm using a UV-vis double beam spectrophotometer. A graph was plotted by taking optical density versus the concentration of TNC used for antibacterial studies (see **Figure 5.20. B**). The nutrient broth-TNC mixture has high optical density for concentrations between $5x10^{-1}$ µg/mL -10 µg/mL due to the bacterial growth; however, at 10 µg/mL of the nanocatalyst, the optical density considerably suppressed due to the inhibition to the growth of the bacterial culture. MIC of TNC was estimated as 10 µg/mL, comparable with the reference range of commercial antimicrobial agents.[77-79] TNC with one-dimensional nanostructure in which silver nanoparticles are attached to MWCNT via less cytotoxic polythiophene layer.[49,57,62a] Silver nanoparticles attached to the nanocomposite can be biocidal by physicochemical interaction with bacterial cells.[26] Comparison study of antibacterial activity of MWCNT-COOH, PTCNT-COOH-300 Ag nanoparticles solution (Ag NPs), BNC, and TNC against *E. coli* bacteria was carried out in lactose broth [lactose broth was selected here to repeat antibacterial activity in another medium] (**see Figure 5.21.**). TNC has shown higher antibacterial activity against *E. Coli* bacteria in the dosage of 10 µg/mL and above. Silver nanoparticles in the dosage of 10 µg/mL have lower antibacterial activity than TNC, which may be due to the aggregation effect of some of the

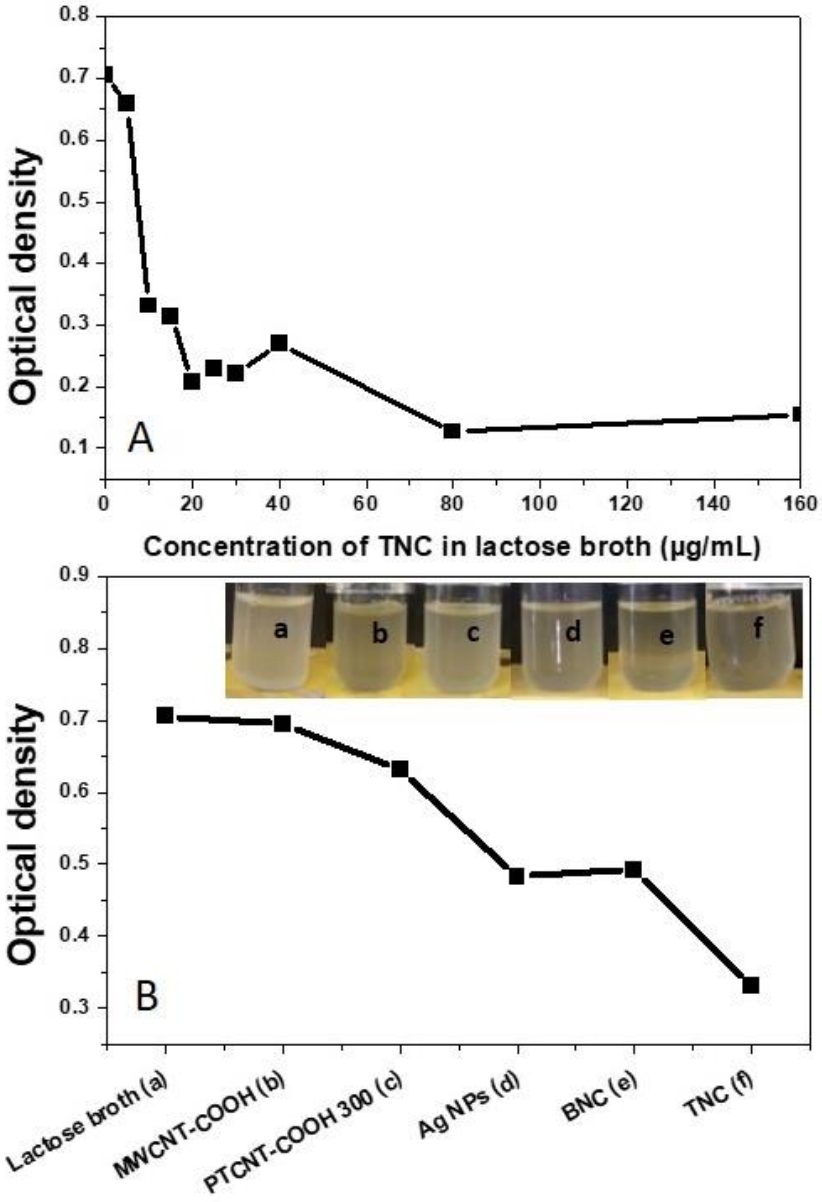

Figure 5.21. *The plot of optical density against the concentration of TNC in lactose broth used in the antibacterial study (A) and plot and photographs of comparison of antibacterial activity of MWCNT-COOH, PTCNT-COOH 300, Ag NPs, BNC and TNC (B).*

Ag NPs during the incubation period. BNC exhibited lower antibacterial activity than that of TNC due to the incapability to maintain stable dispersion for the overnight incubation period. MWCNT-COOH and PTCNT-COOH 300 have no observable antibacterial activity in these 10 µg/mL - 30 µg/mL concentrations. The well-dispersed state of TNC made them highly competent for bacterial inactivation, good dispersion provides more nano-surface active sites for interacting with bacteria.[48] The properties of excellent water dispersibility and recovering nature could be combined with the high antibacterial activity of TNC;

thereby, it could find unique applications in different applications such as water disinfection, medical fields, and textile industries.[48,49] In this chapter ternary and binary nanocomposites demonstrated with their efficient catalytic activity and antibacterial efficiency. We could also illustare involvement of active hydrogens in catalytic hydrogenation of p-nitrophenol (see **Figure 5.22.)**.

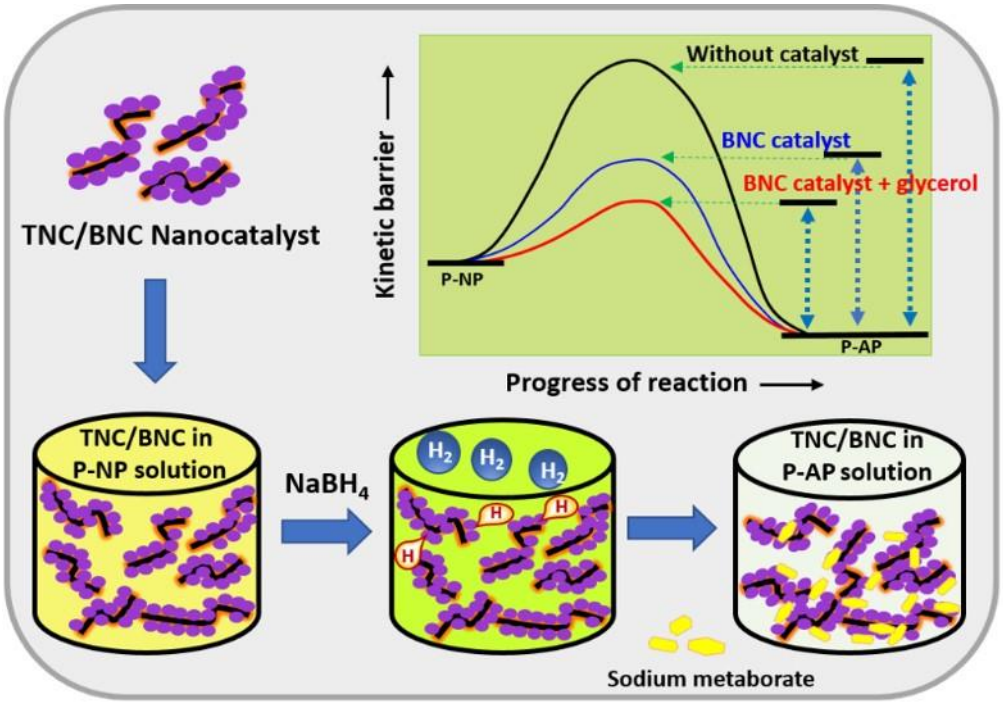

Figure 5.22. *Illustration of involvement of active hydrogens in catalytic hydrogenation of p-nitrophenol*

5.4. Conclusion

We have studied the active solvent hydrogens enhanced catalytic hydrogenation of p-nitrophenol using $NaBH_4$ using two types of heterogeneous silver nanocatalysts. Polymer-supported silver nanoparticles embedded functionalized MWCNT ternary nanocomposites (TNC) and silver nanoparticles directly embedded functionalized MWCNT nanocomposites (BNC). The nanocatalyst BNC was found to exhibit higher catalytic performance than TNC in conversion percentage and recyclable efficiency. Separate control experiments using Ag NPs solution, MWCNT-COOH, and PTCNT-COOH revealed Ag NPs act as a catalyst for the reduction and functionalized multiwalled carbon nanotube (MWCNT-COOH) acts as a supporting framework for stabilizing silver nanoparticles and polythiophene layer to improve the dispersing nature of the

nanocomposites. Comparative study of the kinetics of p-nitrophenol reduction in water and different solvent-water mixtures such as 1,4-dioxane-water, ethanol-water, ethylene glycol-water, and glycerol-water have been demonstrated. The 10 % glycerol-water mixture was an efficient green solvent mixture for the enhanced reduction rate. By utilizing the minimum amount of catalyst (0.005 mg/mL**)** and P-NP: $NaBH_4$ molar ratio 1:200 in a glycerol-water mixture, a fast reduction of p-nitrophenol was obtained with an activity factor of 936.50 s^{-1} g^{-1}. A plausible mechanism of hydrogen source for converting nitro group to amino group by the solvolysis of $NaBH_4$ in a protic solvent has been proposed. Active hydrogens present in the solvent molecules were showing a direct impact on accelerating P-NP reduction using $NaBH_4$. High concentration scale preparation of p-aminophenol by a simple green organic reaction set up with a modest reaction time of one hour has been achieved by reducing p-nitrophenol (1.08×10^{-1} M) using catalyst concentration BNC-0.18 and $NaBH_4$ (2.69 M). The ternary nanocatalyst TNC could also act as an efficient antibacterial agent against the widely used model organism *Escherichia coli* with a minimum concentration of 10 µg/mL.

References

1. Heveling, J. Heterogeneous Catalytic Chemistry by Example of Industrial Applications. *J. Chem. Educ.* **2012**, *89* (12), 1530–1536. https://doi.org/10.1021/ed200816g.
2. Liu, L.; Corma, A. Metal Catalysts for Heterogeneous Catalysis: From Single Atoms to Nanoclusters and Nanoparticles. *Chem. Rev.* **2018**, *118* (10), 4981–5079. https://doi.org/10.1021/acs.chemrev.7b00776.
3. Mizuno, N.; Misono, M. Heterogeneous Catalysis. *Chem. Rev.* **1998**, *98* (1), 199–217. https://doi.org/10.1021/cr960401q.
4. Chandrasekhar, V.; Athimoolam, A. New Hybrid Inorganic-Organic Polymers as Supports for Heterogeneous Catalysis: A Novel Pd(O) Metalated Cyclophosphazene-Containing Polymer as an Efficient Heterogeneous Catalyst for the Heck Reaction. *Org. Lett.* **2002**, *4* (12), 2113–2116. https://doi.org/10.1021/ol026098z.
5. Friend, C. M.; Xu, B. Heterogeneous Catalysis: A Central Science for a Sustainable Future. *Acc. Chem. Res.* **2017**, *50* (3), 517–521. https://doi.org/10.1021/acs.accounts.6b00510.
6. Zhou, Y.; Huang, R.; Ding, F.; Brittain, A. D.; Liu, J.; Zhang, M.; Xiao, M.; Meng, Y.; Sun, L. Sulfonic Acid-Functionalized α-Zirconium Phosphate Single-Layer Nanosheets as a Strong Solid Acid for Heterogeneous Catalysis Applications. *ACS Appl. Mater. Interfaces* **2014**, *6* (10), 7417–7425. https://doi.org/10.1021/am5008408.
7. Shi, J. On the Synergetic Catalytic Effect in Heterogeneous Nanocomposite Catalysts. *Chem. Rev.* **2013**, *113* (3), 2139–2181. https://doi.org/10.1021/cr3002752.
8. Liu, X.; Wen, X.; Hoffmann, R. Surface Activation of Transition Metal Nanoparticles for Heterogeneous Catalysis: What We Can Learn from Molecular Dynamics. *ACS Catal.* **2018**, *8* (4), 3365–3375. https://doi.org/10.1021/acscatal.7b04468.
9. Zhao, P.; Feng, X.; Huang, D.; Yang, G.; Astruc, D. Basic Concepts and Recent Advances in Nitrophenol Reduction by Gold- and Other Transition Metal Nanoparticles. *Coord. Chem. Rev.* **2015**, *287*, 114–136. https://doi.org/10.1016/j.ccr.2015.01.002.

10. Campelo, J. M.; Luna, D.; Luque, R.; Marinas, J. M.; Romero, A. A. Sustainable Preparation of Supported Metal Nanoparticles and Their Applications in Catalysis. *ChemSusChem* **2009**, *2* (1), 18–45. https://doi.org/10.1002/cssc.200800227.
11. Astruc, D. Introduction: Nanoparticles in Catalysis. *Chem. Rev.* **2020**, *120* (2), 461–463. https://doi.org/10.1021/acs.chemrev.8b00696.
12. Deshmukh, S. P.; Dhodamani, A. G.; Patil, S. M.; Mullani, S. B.; More, K. V.; Delekar, S. D. Interfacially Interactive Ternary Silver-Supported Polyaniline/Multiwalled Carbon Nanotube Nanocomposites for Catalytic and Antibacterial Activity. *ACS Omega* **2020**, *5* (1), 219–227. https://doi.org/10.1021/acsomega.9b02526.
13. Alshehri, S. M.; Almuqati, T.; Almuqati, N.; Al-Farraj, E.; Alhokbany, N.; Ahamad, T. Chitosan Based Polymer Matrix with Silver Nanoparticles Decorated Multiwalled Carbon Nanotubes for Catalytic Reduction of 4-Nitrophenol. *Carbohydr. Polym.* **2016**, *151*, 135–143. https://doi.org/10.1016/j.carbpol.2016.05.018.
14. Ahmad, S.; Yang, C.; Xie, W.; Deng, Z.; Zhang, H.; Zhao, Y.; Su, X. Molten Salt-Templated Synthesis of Ternary NiS–NiCo2O4@C Composites as High Performance Catalysts for 4-Nitro Phenol Reduction and Supercapacitor. *Carbon N. Y.* **2020**, *158*, 912–921. https://doi.org/10.1016/j.carbon.2019.11.081.
15. Nariya, P.; Das, M.; Shukla, F.; Thakore, S. Synthesis of Magnetic Silver Cyclodextrin Nanocomposite as Catalyst for Reduction of Nitro Aromatics and Organic Dyes. *J. Mol. Liq.* **2020**, *300*. https://doi.org/10.1016/j.molliq.2019.112279.
16. Yang, X.; Jiang, X.; Bashir, M. S.; Kong, X. Z. Preparation of Highly Uniform Polyurethane Microspheres by Precipitation Polymerization and Pd Immobilization on Their Surface and Their Catalytic Activity in 4-Nitrophenol Reduction and Dye Degradation. *Ind. Eng. Chem. Res.* **2020**, *59* (7), 2998–3007. https://doi.org/10.1021/acs.iecr.9b06367.
17. Kibar, G.; Dinç, D. Ş. Ö. In-Situ Growth of Ag on Mussel-Inspired Polydopamine@poly(M-POSS) Hybrid Nanoparticles and Their Catalytic Activity. *J. Environ. Chem. Eng.* **2019**, *7* (5). https://doi.org/10.1016/j.jece.2019.103435.
18. Liao, G.; Zhao, W.; Li, Q.; Pang, Q.; Xu, Z. Novel Poly (Acrylic Acid)-Modified Tourmaline/Silver Composites for Adsorption Removal of Cu(II) Ions and Catalytic Reduction of Methylene Blue in Water. *Chem. Lett.* **2017**, *46* (11), 1631–1634. https://doi.org/10.1246/cl.170785.
19. Liao, G.; Fang, J.; Li, Q.; Li, S.; Xu, Z.; Fang, B. Ag-Based Nanocomposites: Synthesis and Applications in Catalysis. *Nanoscale* **2019**, *11* (15), 7062–7096. https://doi.org/10.1039/c9nr01408j.
20. Liao, G.; Li, Q.; Zhao, W.; Pang, Q.; Gao, H.; Xu, Z. In-Situ Construction of Novel Silver Nanoparticle Decorated Polymeric Spheres as Highly Active and Stable Catalysts for Reduction of Methylene Blue Dye. *Appl. Catal. A Gen.* **2018**, *549*, 102–111. https://doi.org/10.1016/j.apcata.2017.09.034.
21. Liao, G.; Gong, Y.; Zhong, L.; Fang, J.; Zhang, L.; Xu, Z.; Gao, H.; Fang, B. Unlocking the Door to Highly Efficient Ag-Based Nanoparticles Catalysts for NaBH4-Assisted Nitrophenol Reduction. *Nano Res.* **2019**, *12* (10), 2407–2436. https://doi.org/10.1007/s12274-019-2441-5.
22. Sarkar, A. K.; Saha, A.; Midya, L.; Banerjee, C.; Mandre, N.; Panda, A. B.; Pal, S. Cross-Linked Biopolymer Stabilized Exfoliated Titanate Nanosheet-Supported AgNPs: A Green Sustainable Ternary Nanocomposite Hydrogel for Catalytic and Antimicrobial Activity. *ACS Sustain. Chem. Eng.* **2017**, *5* (2), 1881–1891. https://doi.org/10.1021/acssuschemeng.6b02594.
23. Liu, R.; Hou, Y.; Jiang, S.; Nie, B. Ag(I)-Hived Fullerene Microcube as an Enhanced Catalytic Substrate for the Reduction of 4-Nitrophenol and the Photodegradation of Orange G Dye. *Langmuir* **2020**, *36* (19), 5236–5242. https://doi.org/10.1021/acs.langmuir.0c00580.

24. Kolya, H.; Kuila, T.; Kim, N. H.; Lee, J. H. Bioinspired Silver Nanoparticles/Reduced Graphene Oxide Nanocomposites for Catalytic Reduction of 4-Nitrophenol, Organic Dyes and Act as Energy Storage Electrode Material. *Compos. Part B Eng.* **2019**, *173*. https://doi.org/10.1016/j.compositesb.2019.106924.
25. González, A. L.; Noguez, C.; Beránek, J.; Barnard, A. S. Size, Shape, Stability, and Color of Plasmonic Silver Nanoparticles. *J. Phys. Chem. C* **2014**, *118* (17), 9128–9136. https://doi.org/10.1021/jp5018168.
26. Tejamaya, M.; Römer, I.; Merrifield, R. C.; Lead, J. R. Stability of Citrate, PVP, and PEG Coated Silver Nanoparticles in Ecotoxicology Media. *Environ. Sci. Technol.* **2012**, *46* (13), 7011–7017. https://doi.org/10.1021/es2038596.
27. Astruc, D., Lu, F., & Aranzaes, J. R. (2005). Nanoparticles as recyclable catalysts: The frontier between homogeneous and heterogeneous catalysis. *Angewandte Chemie - International Edition*, *44*(48), 7852–7872. https://doi.org/10.1002/anie.200500766
28. Yu, B.; Han, B.; Jiang, X.; Zhou, C.; Xia, K.; Gao, Q.; Wu, J. Toward High Activity and Durability: An Oxygen-Rich Boron Nitride-Supported Au Nanoparticles for 4-Nitrophenol Hydrogenation. *J. Phys. Chem. C* **2019**, *123* (16), 10389–10397. https://doi.org/10.1021/acs.jpcc.9b00600.
29. Lee, J. W.; Cho, J. Y.; Kim, M. J.; Kim, J. H.; Park, J. H.; Jeong, S. Y.; Seo, S. H.; Lee, G. W.; Jeong, H. J.; Han, J. T. Synthesis of Silver Nanoparticles Embedded with Single-Walled Carbon Nanotubes for Printable Elastic Electrodes and Sensors with High Stability. *Sci. Rep.* **2021**, *11* (1). https://doi.org/10.1038/s41598-021-84386-4.
30. (a) Shifrina, Z. B.; Matveeva, V. G.; Bronstein, L. M. Role of Polymer Structures in Catalysis by Transition Metal and Metal Oxide Nanoparticle Composites. *Chem. Rev.* **2020**, *120* (2), 1350–1396. https://doi.org/10.1021/acs.chemrev.9b00137. (b) Bilalis, P.; Katsigiannopoulos, D.; Avgeropoulos, A.; Sakellariou, G. Non-Covalent Functionalization of Carbon Nanotubes with Polymers. *RSC Adv.* **2014**, *4* (6), 2911–2934. https://doi.org/10.1039/c3ra44906h.
31. Zahed, B.; Hosseini-Monfared, H. A Comparative Study of Silver-Graphene Oxide Nanocomposites as a Recyclable Catalyst for the Aerobic Oxidation of Benzyl Alcohol: Support Effect. *Appl. Surf. Sci.* **2015**, *328*, 536–547. https://doi.org/10.1016/j.apsusc.2014.12.078.
32. Baruah, B.; Gabriel, G. J.; Akbashev, M. J.; Booher, M. E. Facile Synthesis of Silver Nanoparticles Stabilized by Cationic Polynorbornenes and Their Catalytic Activity in 4-Nitrophenol Reduction. *Langmuir* **2013**, *29* (13), 4225–4234. https://doi.org/10.1021/la305068p.
33. Gangu, K. K.; Maddila, S.; Jonnalagadda, S. B. A Review on Novel Composites of MWCNTs Mediated Semiconducting Materials as Photocatalysts in Water Treatment. *Sci. Total Environ.* **2019**, *646*, 1398–1412. https://doi.org/10.1016/j.scitotenv.2018.07.375.
34. Liao, G.; Gong, Y.; Zhang, L.; Gao, H.; Yang, G. J.; Fang, B. Semiconductor Polymeric Graphitic Carbon Nitride Photocatalysts: The "Holy Grail" for the Photocatalytic Hydrogen Evolution Reaction under Visible Light. *Energy Environ. Sci.* **2019**, *12* (7), 2080–2147. https://doi.org/10.1039/c9ee00717b.
35. Ali, G. A. M.; Megiel, E.; Cieciórski, P.; Thalji, M. R.; Romański, J.; Algarni, H.; Chong, K. F. Ferrocene Functionalized Multi-Walled Carbon Nanotubes as Supercapacitor Electrodes. *J. Mol. Liq.* **2020**, *318*. https://doi.org/10.1016/j.molliq.2020.114064.
36. Zhan, W.; Yu, S.; Gao, L.; Wang, F.; Fu, X.; Sui, G.; Yang, X. Bioinspired Assembly of Carbon Nanotube into Graphene Aerogel with "Cabbagelike" Hierarchical Porous Structure for Highly Efficient Organic Pollutants Cleanup. *ACS Appl. Mater. Interfaces* **2018**, *10* (1), 1093–1103. https://doi.org/10.1021/acsami.7b15322.
37. Liu, T.; Sun, Y.; Jiang, B.; Guo, W.; Qin, W.; Xie, Y.; Zhao, B.; Zhao, L.; Liang, Z.; Jiang, L. Pd Nanoparticle-Decorated 3D-Printed Hierarchically Porous TiO2Scaffolds for the Efficient Reduction of a Highly Concentrated 4-Nitrophenol Solution. *ACS Appl. Mater. Interfaces* **2020**, *12* (25), 28100–28109. https://doi.org/10.1021/acsami.0c03959.

38. Kästner, C.; Thünemann, A. F. Catalytic Reduction of 4-Nitrophenol Using Silver Nanoparticles with Adjustable Activity. *Langmuir* **2016**, *32* (29), 7383–7391. https://doi.org/10.1021/acs.langmuir.6b01477.
39. Li, Z.; He, M.; Wen, Y.; Zhang, X.; Hu, M.; Li, R.; Liu, J.; Chu, J.; Ma, Z.; Xing, X.; Yu, C.; Wei, Z.; Li, Y. Highly Monodisperse Cu-Sn Alloy Nanoplates for Efficient Nitrophenol Reduction Reaction via Promotion Effect of Tin. *Inorg. Chem.* **2020**, *59* (2), 1522–1531. https://doi.org/10.1021/acs.inorgchem.9b03370.
40. Scholten, J. D.; Leal, B. C.; Dupont, J. Transition Metal Nanoparticle Catalysis in Ionic Liquids. *ACS Catal.* **2012**, *2* (1), 184–200. https://doi.org/10.1021/cs200525e.
41. Shirin, S.; Roy, S.; Rao, A.; Pillai, P. P. Accelerated Reduction of 4-Nitrophenol: Bridging Interaction Outplays Reducing Power in the Model Nanoparticle-Catalyzed Reaction. *J. Phys. Chem. C* **2020**, *124* (35), 19157–19165. https://doi.org/10.1021/acs.jpcc.0c06237.
42. Neal, R. D.; Hughes, R. A.; Sapkota, P.; Ptasinska, S.; Neretina, S. Effect of Nanoparticle Ligands on 4-Nitrophenol Reduction: Reaction Rate, Induction Time, and Ligand Desorption. *ACS Catal.* **2020**, *10* (17), 10040–10050. https://doi.org/10.1021/acscatal.0c02759.
43. Zhao, Y.; Li, R.; Jiang, P.; Zhang, K.; Dong, Y.; Xie, W. Mechanistic Study of Catalytic Hydride Reduction of -NO2 to -NH2 Using Isotopic Solvent and Reducer: The Real Hydrogen Source. *J. Phys. Chem. C* **2019**, *123* (25), 15582–15588. https://doi.org/10.1021/acs.jpcc.9b02684.
44. Fountoulaki, S.; Daikopoulou, V.; Gkizis, P. L.; Tamiolakis, I.; Armatas, G. S.; Lykakis, I. N. Mechanistic Studies of the Reduction of Nitroarenes by NaBH4 or Hydrosilanes Catalyzed by Supported Gold Nanoparticles. *ACS Catal.* **2014**, *4* (10), 3504–3511. https://doi.org/10.1021/cs500379u.
45. Das, R.; Sypu, V. S.; Paumo, H. K.; Bhaumik, M.; Maharaj, V.; Maity, A. Silver Decorated Magnetic Nanocomposite (Fe3O4@PPy-MAA/Ag) as Highly Active Catalyst towards Reduction of 4-Nitrophenol and Toxic Organic Dyes. *Appl. Catal. B Environ.* **2019**, *244*, 546–558. https://doi.org/10.1016/j.apcatb.2018.11.073.
46. Narayanan, R. K.; Devaki, S. J. Brawny Silver-Hydrogel Based Nanocatalyst for Reduction of Nitrophenols: Studies on Kinetics and Mechanism. *Ind. Eng. Chem. Res.* **2015**, *54* (4), 1197–1203. https://doi.org/10.1021/ie5038352.
47. Mogudi, B. M.; Ncube, P.; Meijboom, R. Catalytic Activity of Mesoporous Cobalt Oxides with Controlled Porosity and Crystallite Sizes: Evaluation Using the Reduction of 4-Nitrophenol. *Appl. Catal. B Environ.* **2016**, *198*, 74–82. https://doi.org/10.1016/j.apcatb.2016.05.051.
48. Krystosiak, P.; Tomaszewski, W.; Megiel, E. High-Density Polystyrene-Grafted Silver Nanoparticles and Their Use in the Preparation of Nanocomposites with Antibacterial Properties. *J. Colloid Interface Sci.* **2017**, *498*, 9–21. https://doi.org/10.1016/j.jcis.2017.03.041.
49. Zako, T.; Sakono, M.; Kobayashi, T.; Sörgjerd, K.; Nilsson, K. P. R.; Hammarström, P.; Lindgren, M.; Maeda, M. Cell Interaction Study of Amyloid by Using Luminescent Conjugated Polythiophene: Implication That Amyloid Cytotoxicity Is Correlated with Prolonged Cellular Binding. *ChemBioChem* **2012**, *13* (3), 358–363. https://doi.org/10.1002/cbic.201100467.
50. Moreira, T.; Laia, C. A. T.; Zangoli, M.; Antunes, M.; Di Maria, F.; De Monte, S.; Liscio, F.; Parola, A. J.; Barbarella, G. Semicrystalline Polythiophene-Based Nanoparticles Deposited from Water on Flexible PET/ITO Substrates as a Sustainable Approach toward Long-Lasting Solid-State Electrochromic Devices. *ACS Appl. Polym. Mater.* **2020**, *2* (8), 3301–3309. https://doi.org/10.1021/acsapm.0c00440.
51. Moghayedi, M.; Goharshadi, E. K.; Ghazvini, K.; Ahmadzadeh, H.; Ranjbaran, L.; Masoudi, R.; Ludwig, R. Kinetics and Mechanism of Antibacterial Activity and Cytotoxicity of Ag-RGO Nanocomposite. *Colloids Surfaces B Biointerfaces* **2017**, *159*, 366–374. https://doi.org/10.1016/j.colsurfb.2017.08.001.

52. Murugan, E.; Vimala, G. Effective Functionalization of Multiwalled Carbon Nanotube with Amphiphilic Poly(Propyleneimine) Dendrimer Carrying Silver Nanoparticles for Better Dispersability and Antimicrobial Activity. *J. Colloid Interface Sci.* **2011**, *357* (2), 354–365. https://doi.org/10.1016/j.jcis.2011.02.009.
53. Liao, G.; He, F.; Li, Q.; Zhong, L.; Zhao, R.; Che, H.; Gao, H.; Fang, B. Emerging Graphitic Carbon Nitride-Based Materials for Biomedical Applications. *Prog. Mater. Sci.* **2020**, *112*. https://doi.org/10.1016/j.pmatsci.2020.100666.
54. Liao, G.; Gong, Y.; Yi, C.; Xu, Z. Soluble, Antibaterial, and Anticorrosion Studies of Sulfonated Polystyrene/Polyaniline/Silver Nanocomposites Prepared with the Sulfonated Polystyrene Template. *Chinese J. Chem.* **2017**, *35* (7), 1157–1164. https://doi.org/10.1002/cjoc.201600816.
55. Marambio-Jones, C.; Hoek, E. M. V. A Review of the Antibacterial Effects of Silver Nanomaterials and Potential Implications for Human Health and the Environment. *J. Nanoparticle Res.* **2010**, *12* (5), 1531–1551. https://doi.org/10.1007/s11051-010-9900-y.
56. Gozdziewska, M.; Cichowicz, G.; Markowska, K.; Zawada, K.; Megiel, E. Nitroxide-Coated Silver Nanoparticles: Synthesis, Surface Physicochemistry and Antibacterial Activity. *RSC Adv.* **2015**, *5* (72), 58403–58415. https://doi.org/10.1039/c5ra09366j.
57. Swathy, T. S.; Jinish Antony, M. Tangled Silver Nanoparticles Embedded Polythiophene-Functionalized Multiwalled Carbon Nanotube Nanocomposites with Remarkable Electrical and Thermal Properties. *Polymer (Guildf).* **2020**, *189*. https://doi.org/10.1016/j.polymer.2020.122171.
58. Wang, Z.; Xu, C.; Gao, G.; Li, X. Facile Synthesis of Well-Dispersed Pd-Graphene Nanohybrids and Their Catalytic Properties in 4-Nitrophenol Reduction. *RSC Adv.* **2014**, *4* (26), 13644–13651. https://doi.org/10.1039/c3ra47721e.
59. Feng, Y.; Yin, J.; Liu, S.; Wang, Y.; Li, B.; Jiao, T. Facile Synthesis of Ag/Pd Nanoparticle - Loaded Poly(Ethylene Imine) Composite Hydrogels with Highly Efficient Catalytic Reduction of 4-Nitrophenol. *ACS Omega* **2020**, *5* (7), 3725–3733. https://doi.org/10.1021/acsomega.9b04408.
60. Liao, G.; Chen, J.; Zeng, W.; Yu, C.; Yi, C.; Xu, Z. Facile Preparation of Uniform Nanocomposite Spheres with Loading Silver Nanoparticles on Polystyrene-Methyl Acrylic Acid Spheres for Catalytic Reduction of 4-Nitrophenol. *J. Phys. Chem. C* **2016**, *120* (45), 25935–25944. https://doi.org/10.1021/acs.jpcc.6b09356.
61. Gu, S.; Wunder, S.; Lu, Y.; Ballauff, M.; Fenger, R.; Rademann, K.; Jaquet, B.; Zaccone, A. Kinetic Analysis of the Catalytic Reduction of 4-Nitrophenol by Metallic Nanoparticles. *J. Phys. Chem. C* **2014**, *118* (32), 18618–18625. https://doi.org/10.1021/jp5060606.
62. (a) Kaloni, T. P.; Giesbrecht, P. K.; Schreckenbach, G.; Freund, M. S. Polythiophene: From Fundamental Perspectives to Applications. *Chem. Mater.* **2017**, *29* (24), 10248–10283. https://doi.org/10.1021/acs.chemmater.7b03035. (b) Swathy, T. S.; Jose, M. A.; Antony, M. J. AOT Assisted Preparation of Ordered, Conducting and Dispersible Core-Shell Nanostructured Polythiophene – MWCNT Nanocomposites. *Polymer (Guildf).* **2016**, *103*, 206–213. https://doi.org/10.1016/j.polymer.2016.09.047. (c) Jose, M. A., Varghese, S., Antony, M. J., (2016). In situ chemical oxidative polymerisation for ordered conducting polythiophene nanostructures in presence of dioctyl sodium sulfosuccinate. Indian Journal of Chemistry, 55A. 292-297
63. Pozun, Z. D.; Rodenbusch, S. E.; Keller, E.; Tran, K.; Tang, W.; Stevenson, K. J.; Henkelman, G. A Systematic Investigation of p -Nitrophenol Reduction by Bimetallic Dendrimer Encapsulated Nanoparticles. *J. Phys. Chem. C* **2013**, *117* (15), 7598–7604. https://doi.org/10.1021/jp312588u.
64. Ortiz-Quiñonez, J. L.; Pal, U. Borohydride-Assisted Surface Activation of Co3O4/CoFe2O4 Composite and Its Catalytic Activity for 4-Nitrophenol Reduction. *ACS Omega* **2019**, *4* (6), 10129–10139. https://doi.org/10.1021/acsomega.9b00118.
65. Chen, W.; Ouyang, L. Z.; Liu, J. W.; Yao, X. D.; Wang, H.; Liu, Z. W.; Zhu, M. Hydrolysis and Regeneration of Sodium Borohydride (NaBH4) – A Combination of Hydrogen

Production and Storage. *J. Power Sources* **2017**, *359*, 400–407. https://doi.org/10.1016/j.jpowsour.2017.05.075.
66. (a) Schlesinger, H. I.; Brown, H. C.; Finholt, A. E.; Gilbreath, J. R.; Hoekstra, H. R.; Hyde, E. K. Sodium Borohydride, Its Hydrolysis and Its Use as a Reducing Agent and in the Generation of Hydrogen. *J. Am. Chem. Soc.* **1953**, *75* (1), 215–219. https://doi.org/10.1021/ja01097a057. (b) Alhokbany, N.; Ahama, T.; Ruksana; Naushad, M.; Alshehri, S. M. AgNPs Embedded N- Doped Highly Porous Carbon Derived from Chitosan Based Hydrogel as Catalysts for the Reduction of 4-Nitrophenol. *Compos. Part B Eng.* **2019**, *173*. https://doi.org/10.1016/j.compositesb.2019.106950.
67. Åkerlöf, G. Dielectric Constants of Some Organic Solvent-Water Mixtures at Various Temperatures. *J. Am. Chem. Soc.* **1932**, *54* (11), 4125–4139. https://doi.org/10.1021/ja01350a001.
68. Mohsen-Nia, M.; Amiri, H.; Jazi, B. Dielectric Constants of Water, Methanol, Ethanol, Butanol and Acetone: Measurement and Computational Study. *J. Solution Chem.* **2010**, *39* (5), 701–708. https://doi.org/10.1007/s10953-010-9538-5.
69. Jouyban, A.; Soltanpour, S. Prediction of Dielectric Constants of Binary Solvents at Various Temperatures. *J. Chem. Eng. Data* **2010**, *55* (9), 2951–2963. https://doi.org/10.1021/je1000632.
70. Brown, H. C.; Mead, E. J.; Rao, B. C. S. A Study of Solvents for Sodium Borohydride and the Effect of Solvent and the Metal Ion on Borohydride Reductions. *J. Am. Chem. Soc.* **1955**, *77* (23), 6209–6213. https://doi.org/10.1021/ja01628a044.
71. Wang, W.; Niu, J.; Yang, Z. An Efficient Reduction of Unsaturated Bonds and Halogen-Containing Groups by Nascent Hydrogen over Raney Ni Catalyst. *J. Hazard. Mater.* **2020**, *389*. https://doi.org/10.1016/j.jhazmat.2019.121912.
72. Song, J.; Huang, Z. F.; Pan, L.; Li, K.; Zhang, X.; Wang, L.; Zou, J. J. Review on Selective Hydrogenation of Nitroarene by Catalytic, Photocatalytic and Electrocatalytic Reactions. *Appl. Catal. B Environ.* **2018**, *227*, 386–408. https://doi.org/10.1016/j.apcatb.2018.01.052.
73. Clarke, C. J.; Tu, W. C.; Levers, O.; Bröhl, A.; Hallett, J. P. Green and Sustainable Solvents in Chemical Processes. *Chem. Rev.* **2018**, *118* (2), 747–800. https://doi.org/10.1021/acs.chemrev.7b00571.
74. Kitanosono, T.; Masuda, K.; Xu, P.; Kobayashi, S. Catalytic Organic Reactions in Water toward Sustainable Society. *Chem. Rev.* **2018**, *118* (2), 679–746. https://doi.org/10.1021/acs.chemrev.7b00417.
75. Xiu, Z. M.; Zhang, Q. B.; Puppala, H. L.; Colvin, V. L.; Alvarez, P. J. J. Negligible Particle-Specific Antibacterial Activity of Silver Nanoparticles. *Nano Lett.* **2012**, *12* (8), 4271–4275. https://doi.org/10.1021/nl301934w.
76. Andrews, J. M. Determination of Minimum Inhibitory Concentrations. *J. Antimicrob. Chemother.* **2001**, *48* (SUPPL. 1), 5–16. https://doi.org/10.1093/jac/48.suppl_1.5.
77. Ramalingam, B.; Parandhaman, T.; Das, S. K. Antibacterial Effects of Biosynthesized Silver Nanoparticles on Surface Ultrastructure and Nanomechanical Properties of Gram-Negative Bacteria Viz. Escherichia Coli and Pseudomonas Aeruginosa. *ACS Appl. Mater. Interfaces* **2016**, *8* (7), 4963–4976. https://doi.org/10.1021/acsami.6b00161.
78. Antony, R.; Marimuthu, R.; Murugavel, R. Bimetallic Nanoparticles Anchored on Core-Shell Support as an Easily Recoverable and Reusable Catalytic System for Efficient Nitroarene Reduction. *ACS Omega* **2019**, *4* (5), 9241–9250. https://doi.org/10.1021/acsomega.9b01023.
79. Deshmukh, S. P.; Patil, S. M.; Mullani, S. B.; Delekar, S. D. Silver Nanoparticles as an Effective Disinfectant: A Review. *Mater. Sci. Eng. C* **2019**, *97*, 954–965. https://doi.org/10.1016/j.msec.2018.12.102.